Model for Economic Tipping point Analysis (META) Model Description

July 8, 2024

Contents

Documentation

This document provides a complete description of the META (Model for Economic Tipping point Analysis) model, which is publicly available at `https://github.com/openmodels/META`. It largely reproduces the description provided in Dietz et al. (2021), but includes the various updates since META-2021.

Figures 1 and 2 provide an overview of the model structure. Figure 1 provides a schematic diagram of the climate module. The inputs to the climate module are greenhouse gas (GHG) emissions from exogenous scenarios; the output is the change in global mean surface temperature (GMST). Three tipping points provide positive feedbacks from the increase in GMST to GHG emissions (the permafrost carbon feedback, dissociation of ocean methane hydrates, and Amazon rainforest dieback), while one provides a positive feedback from the increase in GMST to radiative forcing (Arctic sea-ice loss/surface albedo feedback).

Figure 2 provides a schematic diagram of the damages/economic module. The input to the damages/economic module is the change in GMST from the climate module. The output is discounted utility/social welfare. Slowdown of the Atlantic Meridional Overturning Circulation modulates the relationship between global and national mean temperature change. Disintegration of the Greenland and Antarctic Ice Sheets increases sea level rise. Variability of the Indian summer monsoon directly impacts GDP in India due to droughts and floods.

Figure 1: Schematic diagram of the climate module. Blue boxes indicate variables; yellow boxes indicate tipping point modules; orange boxes indicate other modules.

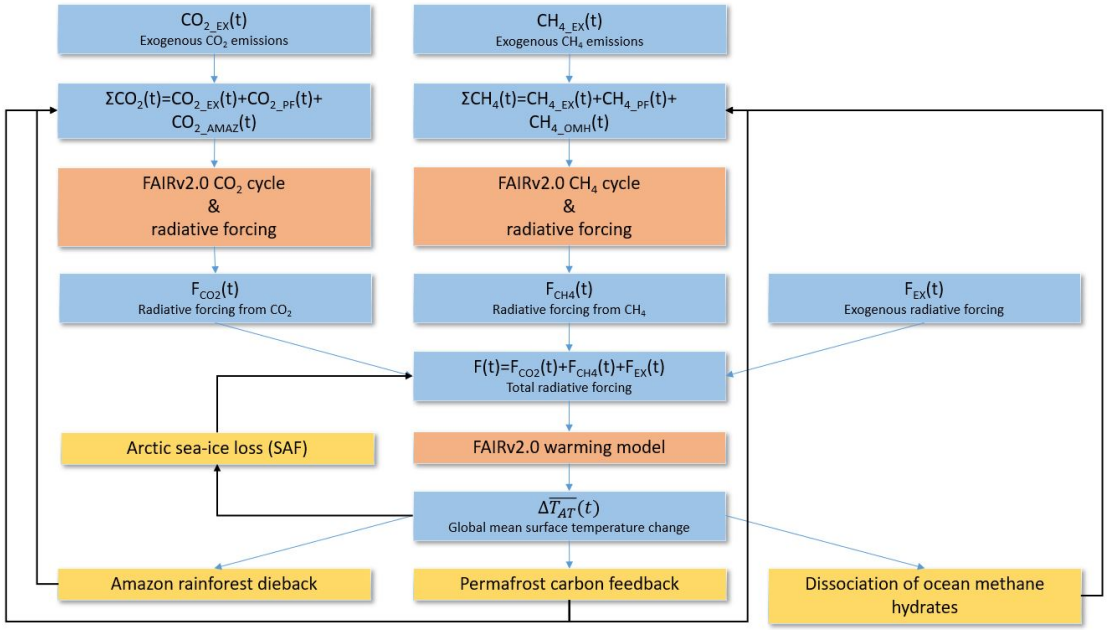

Figure 2: Schematic diagram of the damages/economic module. Blue boxes indicate variables; yellow boxes indicate tipping point modules; orange boxes indicate other modules.

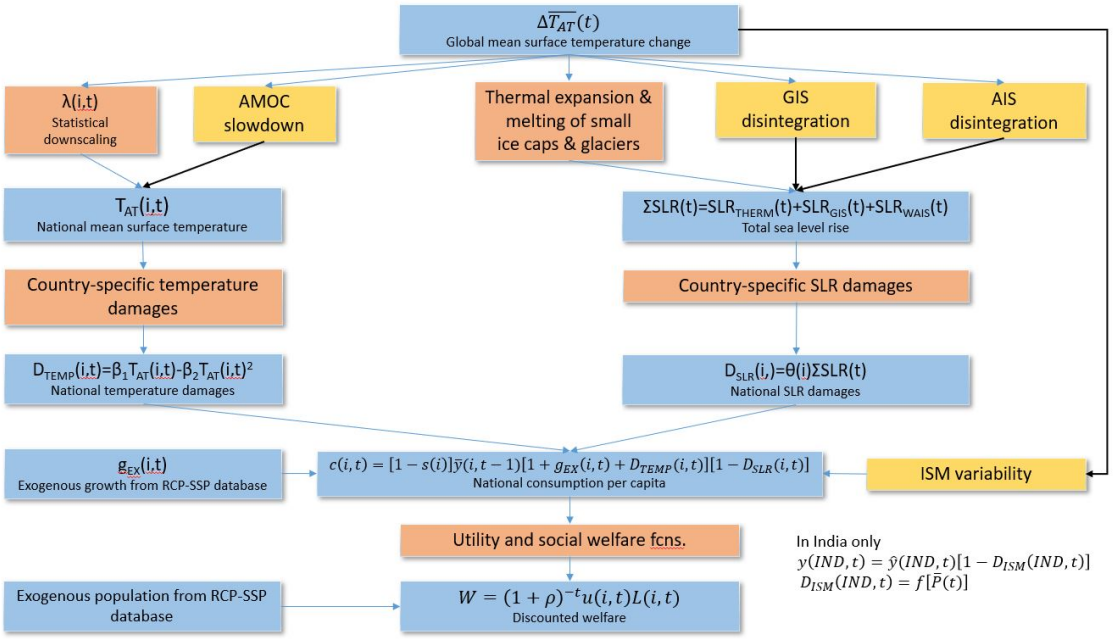

1 Tipping point modules

1.1 Permafrost carbon feedback

Our model of the permafrost carbon feedback (PCF) is taken from Kessler (2017). This is a tractable model that mimics in reduced form the physical-science literature quantifying permafrost carbon release by simulating two stages: (i) permafrost thaw as a function of rising temperatures and (ii) decomposition of thawed permafrost, leading to the release of CO_2 or CH_4. Kessler built the model for incorporation in DICE and, although we don't use DICE, the level of abstraction from the underlying physical processes is well suited to our approach. Despite the level of abstraction, however, the model retains enough structure to be directly calibrated on estimates reported in the underlying literature.

In the first stage, near-surface permafrost thaw is a linear function of warming relative to time zero:

$$\mathrm{PF}_{\mathrm{extent}}(t) = 1 - \beta_{\mathrm{PF}} \left[\Delta\overline{T_{\mathrm{AT}}}(t) - \Delta\overline{T_{\mathrm{AT}}}(0) \right], \tag{1}$$

where $\mathrm{PF}_{\mathrm{extent}}(t) \equiv \mathrm{PF}_{\mathrm{area}}(t)/\mathrm{PF}_{\mathrm{area}}(0)$, i.e., $\mathrm{PF}_{\mathrm{extent}}(t)$ is the area of permafrost remaining at time t relative to time zero, $\Delta\overline{T_{\mathrm{AT}}}$ is the global mean surface air temperature relative to pre-industrial, and β_{PF} is a coefficient representing the sensitivity of permafrost thaw to temperature, which Kessler calibrated by regressing estimates of thaw on temperature from the literature. $t = 0$ in our model is the year 2010.

The amount of carbon in freshly thawed permafrost at time t, C_{thawedPF}, is then the product of the total stock of carbon locked in the near-surface northern circumpolar permafrost region, C_{PF}, and the area of permafrost freshly thawed:

$$C_{\mathrm{thawedPF}}(t) = -C_{\mathrm{PF}} \left[\mathrm{PF}_{\mathrm{extent}}(t) - \mathrm{PF}_{\mathrm{extent}}(t-1) \right]. \tag{2}$$

Once thawed, the principal way in which carbon is released to the atmosphere is microbial decomposition and this happens slowly. Some of the carbon is released as CO_2 and some as CH_4. Kessler's model divides the stock of thawed carbon into a passive reservoir that releases no carbon and an active reservoir that decomposes exponentially and releases CO_2 and CH_4 in fixed proportion. Therefore, cumulative CO_2 emissions to the atmosphere from thawed permafrost, $\mathrm{CCum}_{\mathrm{PF}}$, are given by

$$\mathrm{CCum}_{\mathrm{PF}}(t) = \sum_{s=0}^{t} C_{\mathrm{thawedPF}}(s) \left(1 - \mathrm{propPassive}\right) \left(1 - e^{(-t-s)/\tau}\right), \tag{3}$$

Table 1: PCF model parameter values

	Kessler main spec.	Lower/upper bounds	Fit of Hope and Schaefer (2016)	Fit of Yumashev et al. (2019)
β	0.172	0/1	0.066	0.085
C_{PF} (GtC)	1035	885/1185	1160	1066
propPassive	0.40	0.29/0.51	0.37	0.41
τ (years)	70	0/200	31	66

where propPassive is the proportion of thawed permafrost in the passive reservoir and τ is the e-folding time of permafrost decomposition in the active reservoir, which is multiple decades (see below). The fluxes of CO_2 and CH_4 are respectively given by

$$\mathrm{CO_{2\_PF}}(t) = (1 - \mathrm{propCH_4}) \left[\mathrm{CCum_{PF}}(t) - \mathrm{CCum_{PF}}(t-1)\right], \quad (4)$$

$$\mathrm{CH_{4\_PF}}(t) = (\mathrm{propCH_4}) \left[\mathrm{CCum_{PF}}(t) - \mathrm{CCum_{PF}}(t-1)\right], \quad (5)$$

where $\mathrm{propCH_4}$ is the share of CH_4 emissions in total carbon emissions.

We can directly reproduce the permafrost carbon emissions estimated by Kessler (2017) just by imputing her reported parameter values for β_{PF}, C_{PF}, propPassive, τ and $\mathrm{propCH_4}$ into Equations (1)-(5). In addition, we use this model to fit the results of the two other papers contributed to the IAM literature on the PCF, namely Hope and Schaefer (2016) and Yumashev et al. (2019). Hope and Schaefer (2016) coupled the PAGE09 IAM to the SiBCASA model of the PCF. Yumashev et al. (2019) developed a new version of the PAGE IAM called PAGE-ICE, which includes a representation of the PCF calibrated both on SiBCASA and another PCF model called JULES. We first obtain estimates of permafrost CO_2 emissions from each paper as a function of temperature, and then minimise the sum of squared residuals between these papers' estimates and estimates from Kessler's model, using four of the free parameters in Kessler's model, i.e. β_{PF}, C_{PF}, propPassive, and τ, each parameter restricted to lie within physically plausible bounds. Table 1 reports the various parameter values. Figure 3 shows the fit to cumulative CO_2 emissions from Hope and Schaefer (2016) and Yumashev et al. (2019). CH_4 emissions for these two papers are obtained simply by using the fitted parameters in combination with the fixed value of $\mathrm{propCH_4}$ from Kessler (2017).

Figure 3: Fit of cumulative permafrost CO_2 emissions from Hope and Schaefer (2016), top panel, and Yumashev et al. (2019), bottom panel

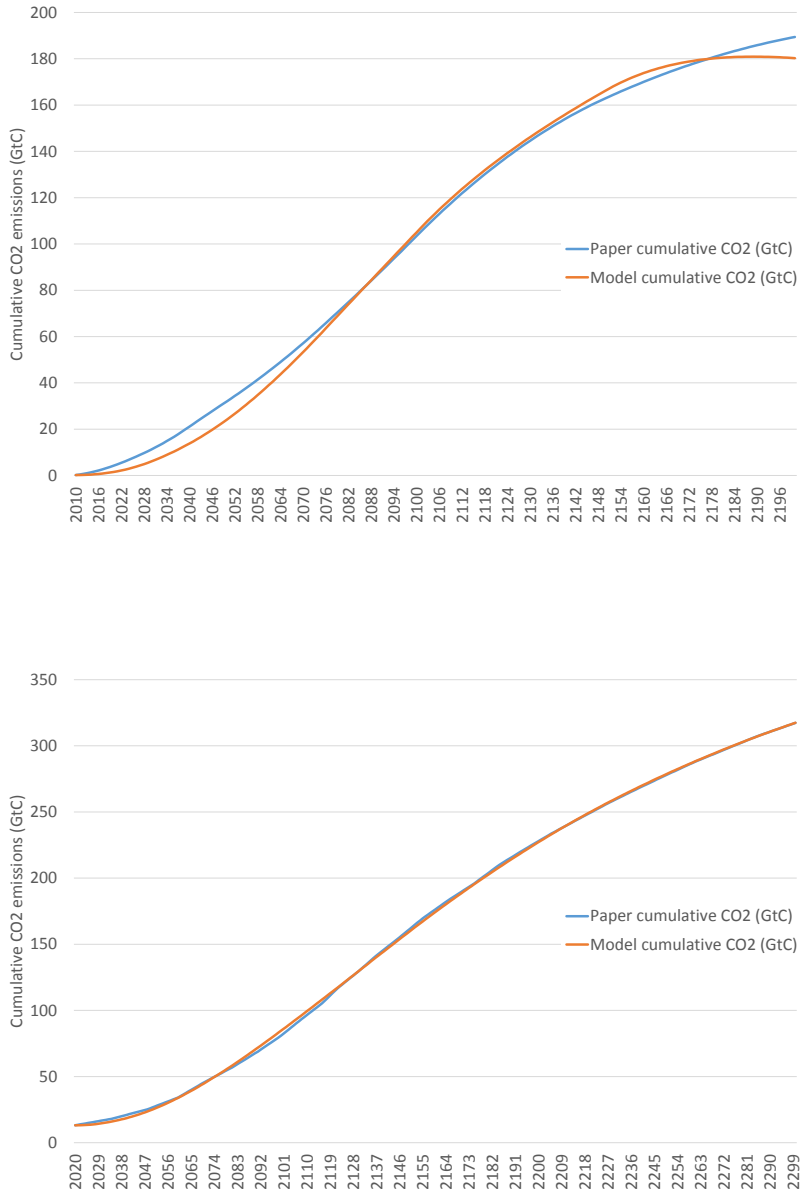

1.2 Ocean methane hydrates

There have been two studies of the economic cost of destabilization of ocean methane clathrates/hydrates. The first is Whiteman, Hope and Wadhams (2013), who implemented what-if scenarios in PAGE09,

releasing a pulse of CH_4 emissions of fixed size and duration into the model at a given point in time. These scenarios were based on the work of Shakhova, Alekseev and Semiletov (2010) on hydrates locked within subsea permafrost on the East Siberian Arctic shelf. Whiteman, Hope and Wadhams (2013) implemented various scenarios. Most of their scenarios involved injecting $50GtCH_4$ in total over periods of 10 to 30 years, starting at different times from 2015 to 2035.[1] The other study is Ceronsky et al. (2011). They implemented three what-if scenarios, in which pulses of CH_4 emissions from the reservoir of CH_4 distributed globally on continental shelves and slopes were released in the FUND IAM. These emissions pulses all commence in 2050 and comprise permanent flows of $0.2GtCH_4$ per year, $1.784GtCH_4$/yr and $7.8GtCH_4$/yr respectively.

In order to incorporate these studies in our analysis, their what-if scenarios need to be assigned probabilities. To do this, we use the framework of survival analysis, treating each emissions pulse as a hazard event and assigning it a hazard rate, i.e. the conditional probability that the event will occur in a particular year, given the temperature in that year and that the event has not occurred previously. This is both convenient, and conforms with the way some of the other studies we synthesise treat tipping points, e.g., on Amazon rainforest dieback (Cai, Lenton and Lontzek, 2016). Once triggered, each CH_4 emissions pulse of given size lasts its pre-specified amount of time. In general, we can write the flow of CH_4 emissions from dissociation of ocean methane hydrates at time t, $\mathrm{CH_{4\_OMH}}(t)$, as

$$\mathrm{CH_{4\_OMH}}(t) = \left(\frac{\overline{\mathrm{CH_{4\_OMH}}}}{\Delta_{\mathrm{OMH}}}\right) I_{\mathrm{OMH}}(t) \quad \Longleftrightarrow \quad \sum_{s=0}^{t-1} \mathrm{CH_{4\_OMH}}(s) < \overline{\mathrm{CH_{4\_OMH}}}, \tag{6}$$

$$\mathrm{CH_{4\_OMH}}(t) = 0 \quad \Longleftarrow \quad \sum_{s=0}^{t-1} \mathrm{CH_{4\_OMH}}(s) = \overline{\mathrm{CH_{4\_OMH}}}, \tag{7}$$

where $\overline{\mathrm{CH_{4\_OMH}}}$ is the pre-specified total amount of methane released, e.g., 50Gt in the case of the main specification of Whiteman, Hope and Wadhams (2013), and Δ_{OMH} is the duration of the release, e.g., 10 years. Applying this formalism to Ceronsky et al. (2011), $\overline{\mathrm{CH_{4\_OMH}}}/\Delta_{\mathrm{OMH}} \in \{0.2, 1.784, 7.8\}$ and total CH_4 released from ocean CH_4 hydrates is bounded only by the product of $\overline{\mathrm{CH_{4\_OMH}}}/\Delta_{\mathrm{OMH}}$ and the model horizon, i.e. the inequality constraint in Equations (6) and (7) does not bind. $I_{\mathrm{OMH}}(t)$ is an indicator function taking a value of zero before the hazard event is triggered and one thereafter. In general, its transition function is

$$I_{\mathrm{OMH}}(t) = f\left[I_{\mathrm{OMH}}(t-1), \Delta\overline{T_{\mathrm{AT}}}(t), \varepsilon(t)\right], \tag{8}$$

[1] They also injected a smaller pulse of $25GtCH_4$ between 2015 and 2025 in one scenario.

where $\varepsilon(t)$ is an i.i.d. random shock. That is, in each period the value of I_{OMH} depends on its own value in the previous period, the current atmospheric temperature, and the random shock. Specifically, the probability transition matrix for $I_{\text{OMH}}(t)$ is

$$\begin{bmatrix} 1 - p_{\text{OMH}}(t) & p_{\text{OMH}}(t) \\ 0 & 1 \end{bmatrix}, \tag{9}$$

where $p_{\text{OMH}}(t)$ is the probability that the CH_4 emissions pulse is triggered in year t. This is given by

$$p_{\text{OMH}}(t) = 1 - \exp\left[-b_{\text{OMH}}\Delta\overline{T_{\text{AT}}}(t)\right], \tag{10}$$

where b_{OMH} is the hazard rate.

In order to calibrate the hazard rate, we use the study of Archer, Buffett and Brovkin (2009), which presents a global model of CH_4 hydrates on continental shelves and slopes and the release of CH_4 as temperatures rise. Their study shows the sensitive dependence of ocean CH_4 release on a critical bubble volume fraction threshold. That is, when ocean CH_4 hydrates melt, it is uncertain whether the CH_4 escapes the ocean sediment into the ocean.[2] Colder temperatures closer to the sea floor and chemical reactions (anaerobic oxidation by bacteria and archaea) both effectively trap the CH_4 from escaping. The more CH_4 is in bubbles, however, the more likely it is to escape. In the model of Archer, Buffett and Brovkin (2009), the bubble volume upon melting of the hydrates must exceed the critical bubble volume fraction in order for the CH_4 to be released. Calibrating the hazard rate on Archer, Buffett and Brovkin (2009) means that we re-interpret Whiteman, Hope and Wadhams (2013) in the context of the global reservoir of CH_4 hydrates on continental shelves and slopes, rather than the reservoir of CH_4 locked in subsea permafrost in the Arctic region. This is justified, since other research suggests a large release of CH_4 from the Arctic subsea permafrost within the next two centuries is extremely unlikely (Archer, 2015).[3]

According to Archer, Buffett and Brovkin (2009), cumulative CH_4 released in very long-run equilibrium upon 1°C warming varies hugely from about 10GtCH_4 to 541GtCH_4 for critical bubble fractions of 10% and 1% respectively.[4] Upon 3°C warming the range increases to about 32-1084Gt. Moreover, Archer, Buffett and Brovkin (2009) report that there is next to no empirical evidence on

[2]There is further uncertainty about whether the CH_4 that reaches the ocean bottom eventually escapes into the atmosphere (it depends on aerobic oxidation of CH_4 by bacteria in the water column), however this uncertainty is thought to be smaller.

[3]Indeed, the scenarios in Whiteman, Hope and Wadhams (2013) were criticised at the time of publication for being unrealistic in the context of Arctic subsea processes; see *Nature* volume 300, p529.

[4]Based on digitising Figure 7 in their paper.

the critical bubble fraction. In the absence of such evidence, we try three alternative specifications of the probability distribution of equilibrium cumulative CH_4 release as a function of the critical bubble fraction (Table 2). The uniform distribution is an application of the principle of insufficient reason. The triangular and especially the beta distribution are more conservative in the sense of assigning more probability mass to higher critical bubble fractions and in turn lower equilibrium CH_4 releases.

Irrespective of the critical bubble fraction, CH_4 released from melting ocean hydrates is thought to take a very long time to reach the atmosphere, much longer than permafrost carbon. Therefore, in order to convert the equilibrium CH_4 release into a transient release, we conservatively assume a release rate of just 0.2%, implying an e-folding time of 500 years and approximately 3,000 years for equilibrium to be reached (also see Archer, Buffett and Brovkin, 2009).

The procedure for calibrating the hazard rate b_{OMH} has been modifed as part of the META model update for this paper. For a given GMST scenario, the approach just described to represent the modelling results of Archer, Buffett and Brovkin (2009) gives us the probability of a cumulative CH_4 release of given volume in a given year. For example, on the mid-range RCP4.5 scenario of the Intergovernmental Panel on Climate Change (IPCC), fed into our climate module excluding tipping points, the middle scenario from Whiteman, Hope and Wadhams (2013) of a cumulative release of $50GtCH_4$ over 20 years from 2015 to 2035 has a probability of 24.4%, assuming a beta distribution over critical bubble fractions. The corresponding hazard rate b_{OMH} is then the value that, given GMST of 1.07°C above pre-industrial in the initial release year of 2015 (also on RCP4.5), triggers the $50GtCH_4$ release with 24.4% probability. In this example, $b_{\text{OMH}} = 0.059$. We follow the same procedure to assign hazard rates using the uniform and triangular distributions, and apply it to different durations of emissions pulse investigated by Whiteman, Hope and Wadhams (2013), as well as the scenarios in Ceronsky et al. (2011). Table 2 reports all the estimated hazard rates. We prefer the beta distributions except in sensitivity analysis, as they are more conservative.

Table 2: Calibration of OMH hazard rate, b_{OMH}. Triangular distribution assumes modal critical bubble fraction of 10%, supports of 1% and zero CH_4 release. Beta distribution assigns cumulative probabilities of 0.67, 0.9, 0.95, 0.99 and 1 to critical bubble fractions of 10%, 7.5%, 5%, 2.5% and 1% respectively.

		uniform	triangular	beta
Whiteman, Hope and Wadhams (2013) 50GtCH$_4$ by 2035	p_{OMH}	95.3%	90.2%	24.4%
	b_{OMH}	0.648	0.491	0.059
Whiteman, Hope and Wadhams (2013) 50GtCH$_4$ by 2025	p_{OMH}	86.4%	8.9%	12.0%
	b_{OMH}	0.422	0.020	0.027
Whiteman, Hope and Wadhams (2013) 50GtCH$_4$ by 2045	p_{OMH}	97.7%	97.8%	33.0%
	b_{OMH}	0.801	0.811	0.084
Ceronsky et al. (2011) 0.2GtCH$_4$/yr 2050-2200	p_{OMH}	100%	100%	67.1%
	b_{OMH}	0.133	0.205	0.019
Ceronsky et al. (2011) 1.784GtCH$_4$/yr 2050-2200	p_{OMH}	99.7%	100%	52.4%
	b_{OMH}	0.096	0.131	0.013
Ceronsky et al. (2011) 7.8GtCH$_4$/yr 2050-2200	p_{OMH}	98.5%	99.2%	39.1%
	b_{OMH}	0.071	0.081	0.008

1.3 Amazon rainforest dieback

Dieback of the Amazon rainforest was included in the study of Cai, Lenton and Lontzek (2016) as a carbon-cycle feedback. This is the study we incorporate in our analysis. Naturally a wide range of other economically important consequences of Amazon rainforest dieback are thereby excluded, including those on biodiversity, ecosystems, and precipitation patterns. These have yet to be incorporated in any economic modelling study, to the best of our knowledge.

As mentioned above, Cai, Lenton and Lontzek (2016) model tipping points through survival analysis. In the case of Amazon rainforest dieback, 50GtC is released over 50 years upon triggering the hazard event. Using parallel formalism to ocean methane hydrates, CO_2 emissions from Amazon rainforest dieback at time t, $\text{CO}_{2\_\text{AMAZ}}(t)$, are given by

$$\text{CO}_{2\_\text{AMAZ}}(t) = \left(\frac{\overline{\text{CO}_{2\_\text{AMAZ}}}}{\Delta_{\text{AMAZ}}}\right) I_{\text{AMAZ}}(t) \quad \Longleftrightarrow \quad \sum_{s=0}^{t-1} \text{CO}_{2\_\text{AMAZ}}(s) < \overline{\text{CO}_{2\_\text{AMAZ}}}, \tag{11}$$

$$\text{CO}_{2\_\text{AMAZ}}(t) = 0 \quad \Longleftarrow \quad \sum_{s=0}^{t-1} \text{CO}_{2\_\text{AMAZ}}(s) = \overline{\text{CO}_{2\_\text{AMAZ}}}, \tag{12}$$

where $\overline{\text{CO}_{2\_\text{AMAZ}}}$ = 50GtC and Δ_{AMAZ} = 50 years. The probability of the indicator function

$I_{\text{AMAZ}}(t)$ transitioning from zero to one is

$$p_{\text{AMAZ}}(t) = 1 - \exp\left[-b_{\text{AMAZ}}\Delta\overline{T_{\text{AT}}}(t) - 1\right], \tag{13}$$

where the hazard rate $b_{\text{AMAZ}} = 0.00163$ in Cai, Lenton and Lontzek (2016) is taken from the expert elicitation study of Kriegler et al. (2009*a*).

1.4 Greenland Ice Sheet

Our model of disintegration of the Greenland Ice Sheet (GIS) is based on Nordhaus (2019), which follows an approach conceptually similar to Kessler's (2017) PCF model by building a simple, reduced-form process model of GIS disintegration for incorporation in DICE.[5] The GIS model is calibrated on results from the underlying literature modelling ice-sheet dynamics. At the heart of the GIS model is the very long-run equilibrium relationship between atmospheric temperature and the volume of the GIS. Assuming this is reversible, Nordhaus (2019) specified

$$\overline{\Delta T^{*}_{\text{GIS}}}(t) = \Delta\overline{T_{\text{GIS\_MAX}}}\left[1 - V_{\text{GIS}}(t)\right], \tag{14}$$

where $\Delta\overline{T^{*}_{\text{GIS}}}(t)$ is defined as the atmospheric temperature increase relative to initial temperature that is associated with a particular degree of melting of the GIS in equilibrium and $V_{\text{GIS}}(t) \in [0, 1]$ is the volume of the GIS expressed as a fraction of the initial volume.[6] In Nordhaus' main specification, Eq. (14) was calibrated on paleoclimatic data from Alley et al. (2010), which gives $\Delta\overline{T_{\text{GIS\_MAX}}} = 3.4$ and implies that the GIS is fully melted in equilibrium when the global mean surface temperature is 3.4°C above pre-industrial. If Robinson, Calov and Ganopolski (2012) is used for calibration instead, $\Delta\overline{T_{\text{GIS\_MAX}}} = 1.8$.[7] An alternative, cubic specification of the equilibrium temperature-volume relationship allows for hysteretic behaviour. Fitted on Alley et al. (2010), this is given by

$$\Delta\overline{T^{*}_{\text{GIS}}}(t) = \Delta\overline{T_{\text{GIS\_MAX}}} - 20.51V_{\text{GIS}}(t) + 51.9\left[V_{\text{GIS}}(t)\right]^2 - 34.79\left[V_{\text{GIS}}(t)\right]^3. \tag{15}$$

Nordhaus (2019) showed that the change in specification makes little difference on the optimal emissions path, which involves relatively limited warming, but can make a difference on high-

[5] The resulting model is called DICE-GIS and builds on DICE-2016R2.

[6] Nordhaus (2019) also reports runs in which $T^{*}_{\text{GIS}}(t) = T_{\text{GIS\_MAX}}\left[1 - V_{\text{GIS}}(t)\right]^{0.5}$ and finds the results are very similar.

[7] Noting that the melt rate coefficient β_{GIS} below also needs to be recalibrated to -0.0000088 to fit Robinson, Calov and Ganopolski (2012).

emissions scenarios.

The difference equation for $V_{\text{GIS}}(t)$, i.e. the GIS melt rate, can be written as

$$\begin{aligned} V_{\text{GIS}}(t) - V_{\text{GIS}}(t-1) &= \beta_{GIS}\text{sgn}\left[\Delta\overline{T_{\text{AT}}}(t-1) - \Delta\overline{T^*_{\text{GIS}}}(t-1)\right] \times \\ &\quad \times \left[\Delta\overline{T_{\text{AT}}}(t-1) - \Delta\overline{T^*_{\text{GIS}}}(t-1)\right]^2 V_{\text{GIS}}(t-1)^{0.2}, \end{aligned} \tag{16}$$

where $\beta_{GIS} = -0.0000106$ based on regression analysis of estimates from Robinson, Calov and Ganopolski (2012).[8] The basic idea embodied in Eq. (16) is that melting of the GIS depends on the difference between the actual atmospheric temperature and the equilibrium GIS temperature, as well as the volume of the GIS at the time.

Sea level rises linearly in response to GIS melt,

$$SLR_{\text{GIS}}(t) = 7\left[1 - V_{\text{GIS}}(t)\right], \tag{17}$$

where SLR_{GIS} is defined relative to the year 2000. This implies that complete disintegration of the GIS would increase global mean sea level by 7 metres.

1.5 Antarctic Ice Sheet

In the latest version of META, melting of the Antarctic Ice Sheet (AIS) is based on a module developed by Dietz and Koninx (2022). This takes a process-based approach. The contribution of the AIS to SLR is divided into the surface mass balance (SMB) contribution and the dynamic contribution. SMB is the balance of surface mass accumulation (precipitation) and ablation (melting) on the ice sheet. Dynamic contributions come from the physical transportation of grounded ice into the ocean through glacier flow. Once afloat, this ice contributes to SLR through the displacement of water. Dynamic contributions are much more important than SMB on the AIS (Garbe et al., 2020).

SMB is modelled using a simple, adjusted linear relationship between SMB and global mean temperature change. The unadjusted annual mass change ΔSMB is given by

$$\Delta\text{SMB} = \gamma\,(t - t_0)^{-0.1}\,\Delta A(t), \tag{18}$$

[8] This corresponds with Nordhaus' Nordhaus (2019) reported value per five years divided by 5 to bring it into line with our annual time step, then divided by 100 given that we define $V_{\text{GIS}}(t)$ as a fraction.

where t_0 is 2010 and $\gamma = 7.95$mm/yr (Frieler et al., 2015). $\Delta A(t)$ is the change in continental-scale accumulation from 2010, which is given by

$$\Delta A(t) = \varphi\omega \left[\Delta\overline{T_{\mathrm{AT}}}(t) - \Delta\overline{T_{\mathrm{AT}}}(0)\right], \tag{19}$$

where φ is a temperature scaling coefficient of 1.2 that converts $\Delta\overline{T_{\mathrm{AT}}}(t)$ into continental-scale temperature change based on the modelling of Garbe et al. (2020), and ω is the change in continental accumulation per degree of Antarctic warming, estimated by Frieler et al. (2015) at approximately 5 +/- 1% per degree warming. We calibrate a normal distribution with a mean of 5% and a standard deviation of 0.4 percentage points.

Equations (18) and (19) permit estimation of the snowfall-induced mass gain for any scenario of global mean temperature change, without needing to rely on runs of a complex ice sheet model. However, Frieler et al. (2015) only analysed the relationship for continental-scale warming of up to 5°C above pre-industrial and temperatures could increase to the extent that SMB in Antarctica turns negative. Garbe et al. (2020) report that the SMB of the ice sheet will turn negative at approx. 7°C warming. To account for this, we model an evolving adjustment factor based on a generalized logistic function:

$$\mathrm{Adjustment}(t) = \frac{K - \Delta\mathrm{SMB}(t)}{\left(C + Qe^{-B(t)}\right)^{1/V}}, \tag{20}$$

where K, C, Q and V are constants, and $B(t) = \left[\Delta\overline{T_{\mathrm{AT}}}(t) - 6.75\right]$. K is calibrated so that the SMB contribution approaches a maximum of 8mm/yr at very high temperatures. This value follows the prognosis from Garbe et al. (2020) that, above c. 7°C warming, the AIS is committed to losing 70% of its mass via the surface elevation feedback. Seventy percent of AIS mass is equivalent to c. 40m of SLR and taking a rapid deglaciation of approximately 5,000 years yields a maximum of 8mm/yr SLR.

Combining (18) and (19) with the adjustment factor and cumulating over time yields the adjusted total mass change:

$$\widehat{\mathrm{SMB}}(t) = \sum_{s=0}^{t} \left[\Delta\mathrm{SMB}(s) + \frac{K - \Delta\mathrm{SMB}(s)}{\left(C + Qe^{-B(s)}\right)^{1/V}}\right]. \tag{21}$$

Dynamic contributions to SLR from the AIS are modelled using the reduced-form model of

Levermann et al. (2020), which is designed to emulate basal ice shelf melting and the resulting contribution of the AIS to SLR in 16 state-of-the-art ice sheet models. The five major ice basins on the continent are modelled separately: East Antarctica, the Ross Sea, the Amundsen Sea, the Weddell Sea, and the Antarctic Peninsula. This is because the dynamic discharge of one basin minimally affects the dynamic discharge of another. The first step is to translate $\Delta\overline{T_{\mathrm{AT}}}$ into subsurface oceanic warming at the mean depth of the ice shelf base in each of the five basins:

$$\Delta T_0(r,t) = \beta(r)\Delta\overline{T_{\mathrm{AT}}}\,(t-\delta(r))\,. \tag{22}$$

Levermann et al. (2020) derived the scaling coefficients $\beta(r)$ and time-delays $\delta(r)$ from 19 CMIP5 models. Each region of Antarctica thus has 19 possible pairs of scaling coefficients and time delays, drawn at random with equal probability. If $t = 2050$ and $\delta(r) = 30$ years, for example, then the input to Equation (22) is $\Delta\overline{T_{\mathrm{AT}}}$ in 2020.

The second step is to map subsurface ocean warming into enhanced basal ice shelf melting:

$$\Delta M(r,t) = \lambda\Delta T_0(r,t), \tag{23}$$

where the basal melt sensitivity parameter λ is randomly chosen from a uniform distribution with lower and upper bounds of $7\mathrm{ma}^{-1}\mathrm{K}^{-1}$ and $16\mathrm{ma}^{-1}\mathrm{K}^{-1}$ respectively. This interval corresponds to values from experimental observations.

The third step translates the enhanced basal ice shelf melting into ice loss/SLR. This utilises reduced-form response functions, which Levermann et al. (2020) estimated on the behaviour of the 16 ice sheet models. Each ice sheet model was initially subjected to a control run from 1900 to 2100. In this control run, the models were forced with historically observed basal ice shelf melting until 2010 and constant forcing thereafter. After the control run, each ice sheet model was then subjected to an artificial external forcing experiment involving an additional stepwise increase of 8m/yr of basal ice shelf melting. The difference in the dynamic contribution to SLR between the experiment and the control run forms the basis of the response function for the particular model and region. The approach assumes that increasing the magnitude of the forcing by a specific factor will increase the magnitude of the response of the ice sheet by the same factor. However, the temporal evolution of the response is not a linear function of time. Response functions can capture the irregular oscillations of ice sheet dynamics in response to external forcing. One must also assume that over the forcing period the five regions of Antarctica respond independently. Levermann et al.

(2020) showed this is a good assumption. Levermann et al. (2020) also subjected the 16 ice sheet models to forcing experiments of 4m/yr and 16m/yr of additional basal melting and compared these responses to the main 8m/yr experiment. Generally, there was good agreement between the responses to the step increases of different size. SLR from dynamic processes S is given by

$$S(r,t) = \sum_{r=1}^{5} \sum_{s=0}^{t} \Delta M(r,s) R(r,s), \tag{24}$$

where R is the value of the response function at time s, drawn at random from the set of 16 models. The total Antarctic SLR contribution is the sum of (21) and (24).

Levermann et al. (2020) derived response functions for the period 1900 to 2100. The period to 2100 is long enough for many of our purposes in this paper, but not for estimating the social cost of CO_2, as a large portion of the current social cost of CO_2 stems from damages after 2100. Therefore, we developed a method of extrapolating the response functions to 2200 using time-series analysis techniques. This makes tractable the extrapolation problem in the absence of being able to run the ice sheet models themselves. We treat the dynamic contribution to SLR estimated by each ice sheet model over the period 1900 to 2100 as a time series. This is first detrended to achieve stationarity and then the properties of the series are estimated using a moving average function of the first or second order, or an ARMA function of the first or second order, with the model being chosen based on best fit under the Akaike Information Criterion.

1.6 Arctic sea-ice loss/surface albedo feedback

Changes in global ice and snow cover also affect the surface albedo feedback (SAF), increasing net radiative forcing. While these effects are implicitly captured in the equilibrium climate sensitivity (ECS) parameter in simple climate models, i.e., the steady-state increase in temperature in response to a doubling of the atmospheric CO_2 concentration, doing so assumes that the marginal forcing from an increase in temperature is constant across temperatures. However, as the area of ice and snow diminishes, the marginal response for further increases in temperature decreases. This SAF dynamic has been modelled by Yumashev et al. (2019) using PAGE-ICE and we replicate their model here.

Yumashev et al. (2019) use a quadratic fit of the SAF observed across the CMIP5 models, shown in the top panel of Figure 4. This falling SAF curve describes the weakening feedback loop between changes in temperature and changes in albedo. For low levels of warming, the SAF is greater than

the constant value represented in the ECS; as sea-ice and land snow diminish, the feedback effect drops. When sea ice and land snow are absent, the SAF effect is zero. The total radiative forcing due to albedo, however, always increases with temperature, and reaches its maximum when sea ice and land snow are absent.

Figure 4: Variation in surface albedo feedback (SAF) effects as a function of GMST. **Top:** SAF as a function of temperature, in terms of marginal increases in forcing per degree Kelvin. **Middle:** adjusted value of the ECS when SAF forcing is removed. **Bottom:** cumulative forcing from the SAF, as a function of temperature, in Wm^{-2}.

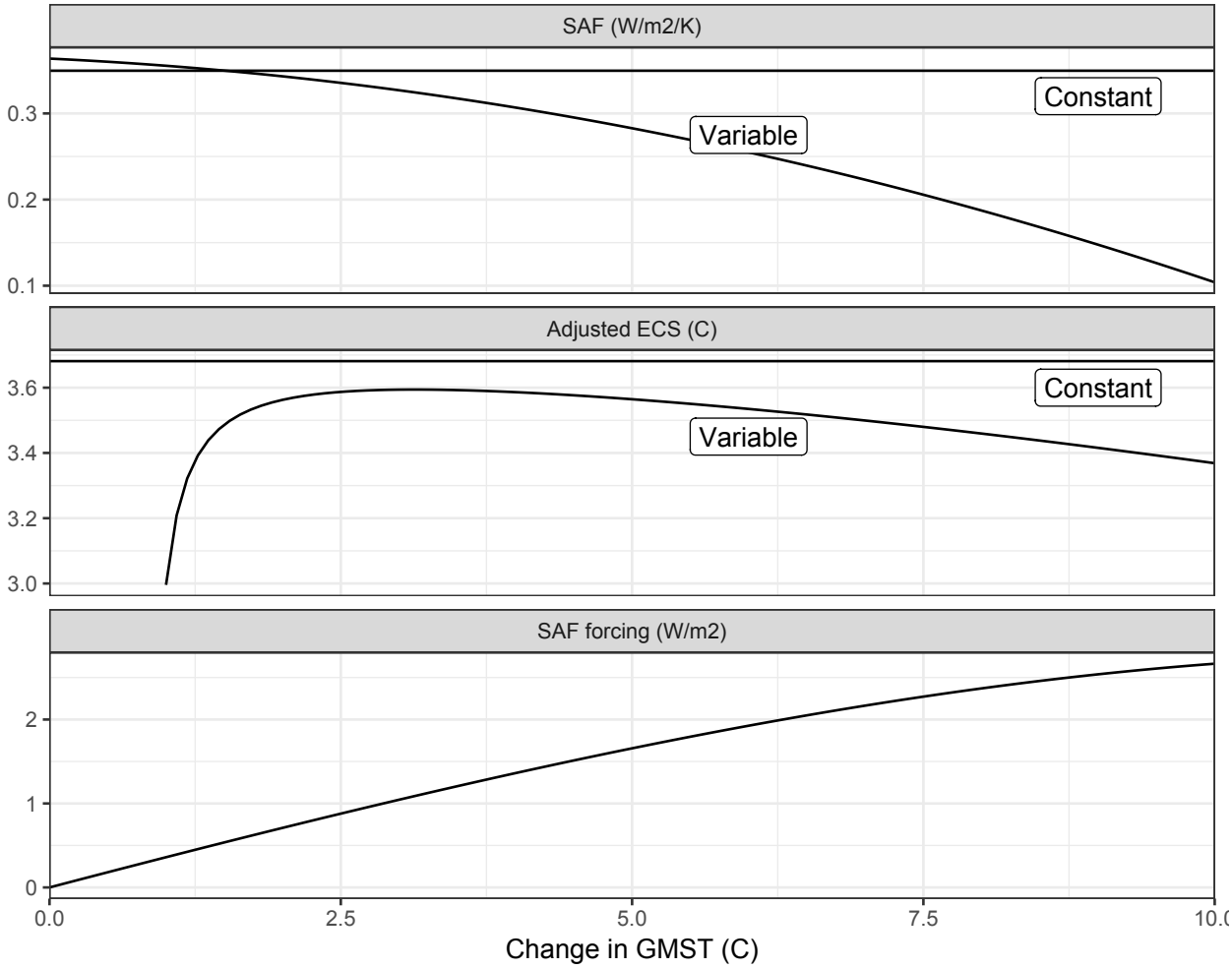

Total SAF forcing is the integral of the SAF feedback effect across the change in temperature, reaching 2.67 Wm^{-2} at warming of 10°C. The ECS follows a non-linear curve calculated as a function of the ECS in the last period, and accounting for the different level of feedback compared to a constant level. As a consequence, adding the SAF to the base climate model can result in lower warming eventually.

The calculations for the SAF correction are shown below. The principle of the SAF model is to correct temperatures calculated under the process used in PAGE-ICE, so we first reproduce this temperature calculation. Global PAGE-ICE atmospheric temperature is calculated as

$$\begin{aligned}\Delta\overline{T_{ATM-PAGE1}}(t) = &\Delta\overline{T_{ATM-PAGE1}}(t-1)\\ &+\left(A(t-1)-\mathrm{FRT}B(t-1)-\Delta\overline{T_{ATM-PAGE1}}(t-1)\right)\left(1-e^{-1/\mathrm{FRT}}\right)\\ &+B(t-1)\end{aligned}$$

where

$$A(t-1)=\frac{\mathrm{ECS}}{F_{sl}\ln 2}F(t-1)$$
$$B(t-1)=\frac{\mathrm{ECS}}{F_{sl}\ln 2}(F(t-1)-F(t-2))$$

$F(t)$ is the anthropogenic forcing in our model

F_{sl} is the forcing slope, 5.5 W/m2

FRT is the warming half-life, from a triangular distribution from 10 to 55 with mode of 20

The surface albedo feedback is then calculated using a quadratic approximation, where SAF decreases more rapidly as temperature increases. The equations are described as an integral over this quadratic:

$$\mathrm{SAF}(t)=\frac{C(\Delta\overline{T_{ATM-PAGE1}}(t))-\mathrm{FSAF}_0}{\Delta\overline{T_{ATM-PAGE1}}(t)-\Delta\overline{T_{ATM-PAGE1}}(2010)}$$

where

$$C(\Delta T)=\beta_2\Delta T^3/3+\beta_1\Delta T^2/2+\beta_0\Delta T+\gamma\Delta T\delta$$

β_2 is the T^2 coefficient for the SAF quadratic ($\mathrm{W/m^2/K^3}$)

β_1 is the T^1 coefficient for the SAF quadratic ($\mathrm{W/m^2/K^2}$)

β_0 is the T^0 coefficient for the SAF quadratic ($\mathrm{W/m^2/K}$)

γ is the standard deviation of the SAF quadratic ($\mathrm{W/m^2/K}$)

δ is the nonlinearity of SAF, drawn from a symmetric triangular distribution from -1 to 1

FSAF_0 is the base year SAF forcing ($\mathrm{W/m^2}$)

The adjustment to the SAF forcing is given by a two-segment correction

$$\Delta\mathrm{FSAF}(t) = -\,\mathrm{SAF}(t)\Delta\overline{T_{ATM-PAGE2}}(t-1) + \begin{cases} C(\Delta\overline{T_{ATM-PAGE2}}(t-1)) & \text{if } \Delta\overline{T_{ATM-PAGE2}}(t-1) < 10 \\ D(\Delta\overline{T_{ATM-PAGE2}}(t-1)) & \text{if } \Delta\overline{T_{ATM-PAGE2}}(t-1) \geq 10 \end{cases}$$

where

$$D(\Delta T) = \psi + \alpha(\Delta T - 10) + \sigma(\Delta T - 10)\delta$$

$\Delta\overline{T_{ATM-PAGE2}}(t)$ is defined below.

ψ is the integration constant for SAF forcing at the segment switch point

α is the linear SAF segment mean

σ is the linear SAF segment standard deviation

Also using $SAF(t)$, the adjusted ECS and FRT values are calculated as

$$\mathrm{ECS}' = \mathrm{ECS}\left(1 - \frac{\mathrm{ECS}\left(\mathrm{SAF}(t) - \overline{SAF}\right)}{F_{sl}\ln 2}\right)^{-1}$$

$$\mathrm{FRT}' = \mathrm{FRT}\left(1 - \frac{\mathrm{ECS}\left(\mathrm{SAF}(t) - \overline{SAF}\right)}{F_{sl}\ln 2}\right)^{-1}$$

where $\overline{SAF}$ is the constant approximation to the SAF (0.34959 W/m^2/C).

Then $\Delta\overline{T_{ATM-PAGE2}}(t)$, the adjusted temperature time-series, is calculated identically to $\Delta\overline{T_{ATM-PAGE1}}(t)$, but using ECS′, FRT′, and with the additional forcing $\Delta\mathrm{FSAF}(t)$. The temperature adjustment produced by the SAF model, $\Delta\overline{T_{ATM-PAGE2}}(t) - \Delta\overline{T_{ATM-PAGE1}}(t)$, is then added to the main temperature in the model.

1.7 Slowdown of the Atlantic Meridional Overturning Circulation

Weakening of the Atlantic Meridional Overturning Circulation (AMOC) or thermohaline circulation,[9] whether partial or full, has inspired a number of numerical modelling studies in climate

[9] We use these two terms interchangeably.

economics (Anthoff, Estrada and Tol, 2016; Bahn et al., 2011; Belaia, Funke and Glanemann, 2017; Ceronsky et al., 2011; Keller, Bolker and Bradford, 2004; Lempert, Sanstad and Schlesinger, 2006; Link and Tol, 2004, 2011; Schlesinger et al., 2006). The majority of these take a stylised approach. Of those aiming for realism, we choose to incorporate the results of Anthoff, Estrada and Tol (2016) in our model, because of their unique focus on the effects of AMOC slowdown at the national level. This is arguably central to the economic evaluation of AMOC slowdown, because its physical effects would vary significantly across the world, from a reduction in regional temperature of several degrees, all else being equal, to an increase in regional temperature of a few tenths of a degree (see Anthoff, Estrada and Tol, 2016, fig. 1). The basic logic is that the ocean circulation redistributes heat, rather than creating or destroying it, and countries vary in their exposure to this heat redistribution, as well as the effects of global warming more broadly, depending on their physical location. AMOC slowdown is expected to have physical effects other than temperature change, for instance effects on precipitation and regional sea levels (Lenton and Ciscar, 2013), but these have yet to be incorporated in economic studies.

Anthoff, Estrada and Tol (2016) implement four what-if scenarios known in the context of AMOC slowdown as 'hosing experiments'. In these experiments, a large exogenous pulse of freshwater is added to the representation of the North Atlantic in General Circulation Models – hence the term hosing – and the consequences for the AMOC are simulated. Note this is additional to any gradual slowdown of AMOC captured by the climate models of CMIP6, which our calibrated pattern scaling of global into national temperatures already captures (see below). The four scenarios result in an AMOC slowdown of 7%, 24%, 27% and 67% respectively. This slowdown is assumed to be reached in the year 2085, after being phased in linearly from a 2050 starting point. As is by now familiar, we convert these what-if scenarios into hazard events and assign them probabilities. The national temperature delta arising from AMOC slowdown is hence given by

$$\begin{aligned}
\Delta T_{\text{AT_AMOC}}(i,t) &= \Delta T_{\text{AT_AMOC}}(i,t-1) + \left(\frac{\overline{\Delta T_{\text{AT_AMOC}}(i)}}{\Delta_{\text{AMOC}}}\right) I_{\text{AMOC}}(t) \\
&\iff \sum_{s=0}^{t-1} \Delta T_{\text{AT_AMOC}}(i,s) < \overline{\Delta T_{\text{AT_AMOC}}(i)}, \qquad (25) \\
\Delta T_{\text{AT_AMOC}}(i,t) &= \overline{\Delta T_{\text{AT_AMOC}}(i)} \\
&\iff \sum_{s=0}^{t-1} \Delta T_{\text{AT_AMOC}}(i,s) = \overline{\Delta T_{\text{AT_AMOC}}(i)}, \qquad (26)
\end{aligned}$$

where $\overline{\Delta T_{\text{AT\_AMOC}}(i)}$ is the permanent difference in national annual average temperature as a result of AMOC slowdown in country i. The data points corresponding to $\overline{\Delta T_{\text{AT\_AMOC}}(i)}$ were kindly provided by Anthoff and colleagues for all countries they covered. Δ_{AMOC} is the time taken for AMOC slowdown to phase in, i.e. 35 years. $I_{\text{AMOC}}(t)$ is the indicator function, whose transition probability from zero to one is

$$p_{\text{AMOC}}(t) = \begin{cases} 1 - \exp\left[-b_{\text{AMOC}}\Delta\overline{T_{\text{AT}}}(t)\right] & \text{if } t = 1 \\ (1 - \exp\left[-b_{\text{AMOC}}\Delta\overline{T_{\text{AT}}}(t)\right]) - (1 - \exp\left[-b_{\text{AMOC}}\Delta\overline{T_{\text{AT}}}(t-1)\right]) & \text{if } t > 1 \end{cases} \tag{27}$$

conditional on $I_{\text{AMOC}}(t-1) = 0$.

To calibrate the hazard rate for each of the four scenarios in Anthoff, Estrada and Tol (2016), we compile likelihoods as a function of global mean temperature increase for distinct AMOC shutdown events ranging from a weakening of 11% to a full shutdown. We obtain these from the IPCC *Fifth Assessment Report* (Stocker et al., 2013), its *Special Report on Global Warming of 1.5°C* (Hoegh-Guldberg et al., 2018), and Gosling (2013). Given the limited measurements of AMOC intensity, these numbers reflect a combination of model-based estimates and expert judgement. We proceed in two steps: (i) we take the convex combination of the AMOC shutdown events from the literature that most closely resembles the what-if scenario at hand. To obtain a hazard rate b_{AMOC}, we then (ii) calibrate Equation (27) by minimizing the sum of squared differences to the likelihoods obtained in step (i). We estimate $b_{\text{AMOC}} = 1.6$ for a 7% slowdown, 0.611 for a 24% slowdown, 0.54 for 27% and 0.135 for 67%.

1.8 Weakening of the Indian Summer Monsoon

The first integrated assessment of the Indian Summer Monsoon (ISM) and its response to climate change has recently been carried out by Belaia (2017). This is based on coupling a version of Nordhaus' regionally disaggregated RICE IAM (Ikefuji, Magnus and Sakamoto, 2014) to a model of the ISM (Schewe and Levermann, 2012). The ISM is driven by greater heating of the land surface relative to the ocean in summer, which creates a pressure gradient that drives moist ocean air over the Indian subcontinent, where it rises and condenses. However, ISM rainfall displays important year-to-year variation and the ISM has the potential to abruptly change regime from wet to dry and *vice versa*. Schewe and Levermann's model generates these dynamics by incorporating reduced-form

representations of two competing feedback processes. The first is the so-called moisture advection feedback, a positive feedback whereby monsoon rains release latent heat, which strengthens the monsoon circulation and brings more rainfall in turn. The second is the dry-subsidence effect, a negative feedback whereby high pressure reduces rainfall, the decreased rainfall leads to less latent heat being released, which in turn sustains the dry phase. High pressure also deflects winds away from the monsoon region. In Belaia (2017)'s model , rainfall depends on both climate change, through multiple channels, and regional emissions of sulphur dioxide, which reflect incoming solar radiation, reduce heating over the Indian subcontinent and weaken the ISM.

The key output of the ISM model that feeds into damages to India (see below) is average rainfall over the Indian subcontinent over the summer monsoon season:

$$\overline{P}(t) = \frac{1}{136}\sum_{d=1}^{136} P(d,t), \tag{28}$$

where $P(d,t)$ is rainfall on day d of year t and there are 136 days in each monsoon season.[10] Each day is either wet or dry, depending on

$$P(d,t) \quad = \quad \begin{cases} P_{\text{wet}}(t), & Pr(d,t) < p(d,t), \\ P_{\text{dry}} & Pr(d,t) \geq p(d,t), \end{cases} \tag{29}$$

where $Pr(d,t) = U(0,1)$, capturing random variation in day-to-day weather. There is no rainfall on a dry day, whereas rainfall on a wet day is an increasing function of atmospheric temperature, since a warmer atmosphere can hold more water:

$$P_{\text{wet}}(t) = p'' \left[\Delta\overline{T_{\text{AT}}}(t) - \Delta\overline{T_{\text{AT}}}(0)\right] + P_{\text{wet}}(0). \tag{30}$$

The initial value of P_{wet} is 9mm per day and it increases by 0.42mm/day/°C of global warming.

The probability of a wet day during the first δ days of the season – the onset – is

$$p_{\text{init}}(t) \quad = \quad \begin{cases} p_{\text{init},1}(t), & A_{\text{pl}}(t) < A_{\text{pl,crit}}(t), \\ 1 - p_{\text{m}}, & A_{\text{pl}}(t) \geq A_{\text{pl,crit}}(t), \end{cases} \tag{31}$$

[10] For computational reasons, we use a four-day time step, so $P(d,t)$ changes at most once every four days and there are 136 days in the season, compared with 135 in Belaia (2017).

where $p_{\mathrm{m}} = 0.82$ is the maximum probability of a wet day.[11] The formulation in Eq. (31) makes rainfall during the onset of the season a function of albedo $A_{\mathrm{pl}}(t)$, in particular its relation to a critical albedo value $A_{\mathrm{pl,crit}}(t)$. If the actual albedo exceeds the critical value, the probability of a wet day is at its minimum. The critical albedo value is increasing in the atmospheric concentration of CO_2,

$$A_{\mathrm{pl,crit}}(t) = \alpha_{\mathrm{pl},1} \ln \left[\sum_{i=0}^{3} S_i(t) + \underline{S} \right] + \alpha_{\mathrm{pl},2}. \tag{32}$$

$\sum_{i=0}^{3} S_i(t) + \underline{S}$ gives the atmospheric CO_2 concentration and its derivation is explained in the following section. The actual albedo is given by

$$A_{\mathrm{pl}}(t) = A_{\mathrm{pl}}(0) + 2T_{\mathrm{pl}}^2(1 - A_{\mathrm{s}})^2 \beta_{\mathrm{pl}} \alpha_{\mathrm{pl},3} B_{\mathrm{SO4}}(t), \tag{33}$$

where T_{pl} is the fraction of light transmitted by the aerosol layer, A_{s} is the present value of the surface albedo, β_{pl} and $\alpha_{\mathrm{pl},3}$ are coefficients representing the backscatter fraction and mass scattering efficiency respectively and $B_{\mathrm{SO4}}(t)$ is the regional sulphate burden over the Indian peninsula. This last quantity depends on SO_2 emissions in the region:

$$B_{\mathrm{SO4}}(t) = \mathrm{SO}_2(t) H_{\mathrm{SO2}} V / \Omega. \tag{34}$$

Emissions of SO_2 are exogenous and sourced from the Representative Concentration Pathway (RCP) database Moss et al. (2010). The emissions scenarios we use are discussed in greater detail below. The RCP database only disaggregates SO_2 emissions to the level of the Asian continent/region, so we downscale to the Indian level by assuming a constant ratio of Indian/Asian emissions, estimated based on 2010 data Li et al. (2017). The parameter H_{SO2} is the fractional sulphate yield, V is the atmospheric lifetime of sulphate and Ω is the land area. Thus the dependence of rainfall on albedo in the model ultimately captures the local cooling effect of SO_2 emissions in the region, which weakens the ISM.

Assuming the actual planetary albedo does not exceed the critical value, the probability of a wet day during the first δ days of the season is

$$p_{\mathrm{init},1}(t) = p' \left[m_{\mathrm{NINO3.4}}(t) - m_0 \right] + p_0, \tag{35}$$

[11] By bounding the probability of a wet day during the onset of the monsoon season, the system does not become irrevocably locked into either a wet or dry state.

where $m_{\text{NINO3.4}}$ is the strength of the Walker circulation, i.e., the Pacific Ocean atmospheric circulation, in May. The subscript NINO indicates that the strength of this circulation depends on whether there is an El Niño or not. El Niño suppresses the ISM. The parameters p', m_0 and p_0 are used to calibrate the response of $p_{\text{init},1}(t)$ to $m_{\text{NINO3.4}}$. The strength of the Walker circulation in May is in turn given by

$$m_{\text{NINO3.4}}(t) = m' \left[\Delta\overline{T_{\text{AT}}}(t) - \Delta\overline{T_{\text{AT}}}(0)\right] + m_{\text{NINO3.4}}(0). \tag{36}$$

The probability of a wet day after the first δ days of the season is

$$p(d,t) = \frac{1/\delta \sum_{i=d-\delta}^{d-1} P(i,t) - P_{\text{dry}}}{P_{\text{wet}}(t) - P_{\text{dry}}}, \tag{37}$$

where $\delta = 16$ days.[12] The probability of a wet day depends positively on how wet the previous δ days were, a representation of the moisture advection and dry-subsidence feedbacks.

1.9 Tipping point interactions

Tipping points can interact with each other in multiple ways (Cai, Lenton and Lontzek, 2016; Kriegler et al., 2009*a*). Some of these interactions are hardwired into the structure of our model. For example, the PCF increases GMST, which affects all seven remaining tipping points in our study, because all of them depend on temperature. However, the structure of our model can only capture a limited subset of all the possible interactions between tipping points. To increase the number of interactions, we use the expert elicitation study of Kriegler et al. (2009*a*), which attempted to quantify how the triggering of one tipping point can cause the hazard rates of other tipping points to change, with a focus on mechanisms other than temperature.

We apply a hierarchical Bayesian analysis to obtain best estimates of the hazard rate changes provided by the experts in Kriegler et al. (2009*a*). The hazard rate changes – the interactions – are represented by a range for expert i from lower bound u_i to upper bound n_i. Each change/interaction is a multiplier on the base hazard rate, so a value of 1 means no change. We posit a true, expert-specific hazard rate change, θ_i, and further assume that these true values are drawn from a normal distribution with unknown mean and variance. This allows the expert opinions to be partially

[12] With a four-day time step, we set the memory period $\delta = 16$ days, rather than 17 days as in Belaia (2017).

pooled to inform the hyperparameters of the normal distribution:

$$\theta_i \sim \mathcal{N}(\mu, \tau)$$
$$\theta_i \sim \mathcal{U}(u_i, n_i)$$

We treat cases where experts were uncertain about the lower bound of the hazard rate change as having a lower bound of 0, and cases where they were uncertain about the upper bound as an upper bound of 10. Figure 5 presents the results.

Figure 5: The posterior distribution of μ, the mean of the hyperdistribution, for each interaction. The error bars in each plot show the 95% credible interval on μ for the given interaction. The light grey lines show each expert's upper and lower bounds (dots are used if the upper bound equals the lower bound). Abbreviations are as follows: Atlantic Meridional Overturning Circulation (AMOC), melt of the Greenland Ice Sheet (GIS), disintegration of the West Antarctic Ice Sheet (WAIS), and dieback of the Amazon rainforest (AMAZ).

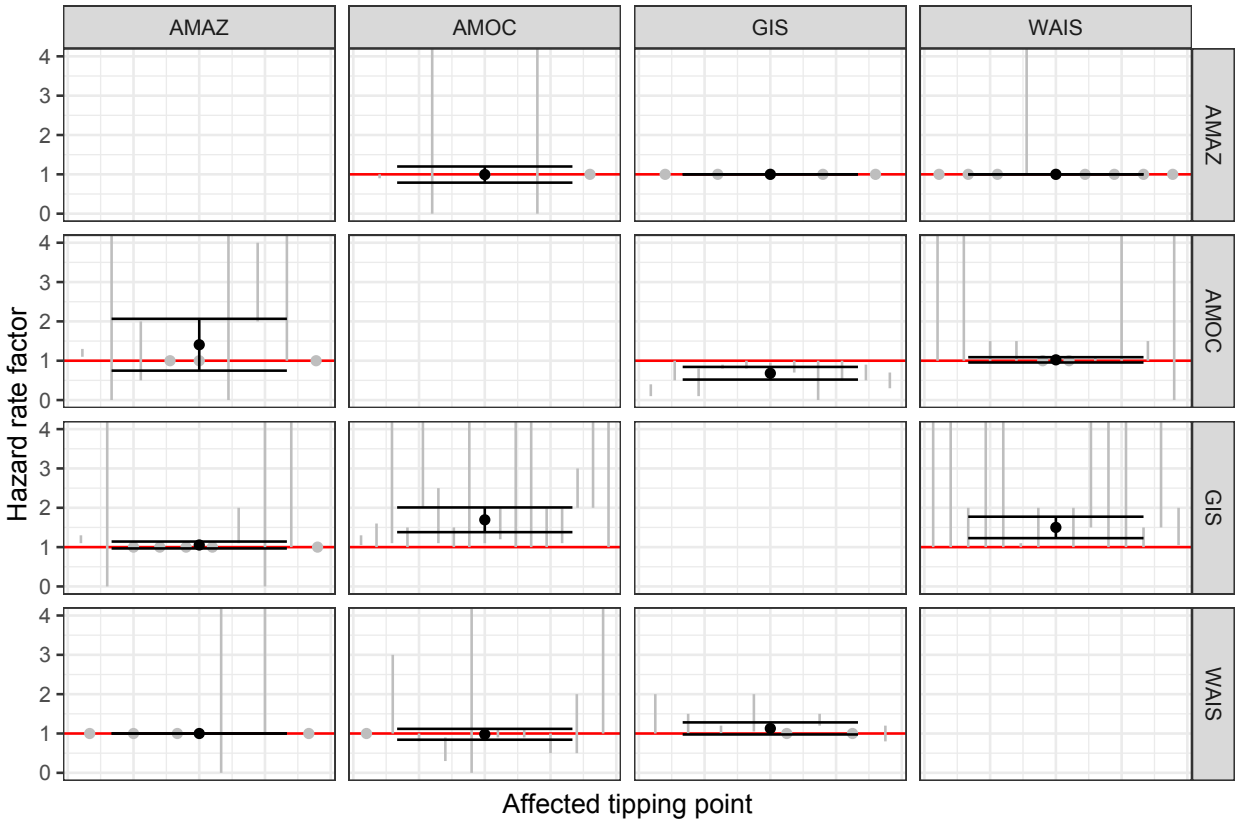

The set of tipping point interactions included in our study is the union of the set of interactions hardwired in our model and the set of interactions quantified by Kriegler et al. (2009*a*). To aid understanding of how many interactions are thereby included, as well as the direction of each

interaction, Table 3 provides a matrix.

Table 3: Interactions between tipping points included in this study. Each cell indicates the qualitative effect of the row tipping point on the column tipping point. Where the row tipping point can increase or decrease the intensity/likelihood of the column tipping point, depending on time or state, we write +/-. Parentheses indicate the interaction is calibrated on the expert elicitation study by Kriegler et al. (2009*a*). The absence of parenthesis indicates the interaction is hardwired in the model structure. Zeros indicate an interaction that is included, but that has a statistical zero effect according to Kriegler et al. (2009*a*). No int. means the interaction is not included at all. n.b. ISM affects other tipping points via ENSO, implicit in the expert estimates of the relevant hazard rate changes. AIS interactions are calibrated on the ice sheet responses of the four Western regions of Antarctica only, to match with the notion of WAIS in Kriegler et al. (2009*b*).

	PCF	OMH	SAF	AMAZ	GIS	AIS	AMOC	ISM
PCF		+	+	+	+	+	+	+/-
OMH	+		+	+	+	+	+	+/-
SAF	+/-	+/-		+/-	+/-	+/-	+/-	+/-
AMAZ	+	+	+		+ (0)	+ (0)	+ (+/-)	+/- (+/-)
GIS	no int.	no int.	no int.	(+/-)		(+)	(+)	(0)
AIS	no int.	no int.	no int.	(0)	(+/-)		(+/-)	(0)
AMOC	no int.	no int.	no int.	(+/-)	(-)	(+/-)		(0)
ISM	no int.	no int.	no int.	(+)	(0)	(0)	(+/-)	

2 Climate module

2.1 Emissions

The principal inputs to the climate model are global emissions of CO_2 and CH_4. Other anthropogenic and natural sources of radiative forcing, both positive and negative, are aggregated into an exogenous residual radiative forcing series.[13] Anthropogenic emissions come from the scenarios described in the scenario section above. The second source of emissions is the carbon-cycle feedbacks described in the previous section, i.e., permafrost melting, dissociation of ocean methane hydrates, and Amazon rainforest dieback.

[13]This is the sum of forcing from: (i) N_2O; (ii) flourinated gases controlled under the Kyoto Protocol; (iii) ozone-depleting substances controlled under the Montreal Protocol; (iv) total direct aerosol forcing; (v) the cloud albedo effect; (vi) stratospheric and tropospheric ozone forcing; (vii) stratospheric water vapour from methane oxidisation; (viii) land-use albedo; (ix) black carbon on snow.

2.2 CO_2 and CH_4 cycles

CO_2 and CH_4 emissions are mapped into atmospheric concentrations using the FaIR simple climate model, version 2.0.0 (Leach et al., 2021), specifically the Julia-Mimi implementation of the model available at https://github.com/FrankErrickson/MimiFAIRv2.jl.git. This updates the CO_2 and CH_4 cycles from META-2021, which were based on FaIRv1.0 (Millar et al., 2017) for CO_2 and our own representation of the CH_4 cycle.

In FaIR, each gas cycle is represented by the following system of equations (sticking with discrete time notation and following closely the Julia-Mimi implementation):

$$C(t) = \underline{C} + \frac{1}{2}\left[\sum_{i=1}^{n} R_i(t-1) + \sum_{i=1}^{n} R_i(t)\right], \tag{38}$$

$$R_i(t) = E(t)\frac{a_i}{\delta_i(t)}\left[1 - e^{-\delta_i(t)}\right] + R_i(t-1)e^{-\delta_i(t)}, \tag{39}$$

$$\delta_i(t) = \frac{1}{\alpha(t)\tau_i}, \tag{40}$$

$$\alpha(t) = g_0 \exp\left(\frac{r_0 + r_u G_u(t-1) + r_T \Delta\overline{T_{AT}}(t-1) + r_a G_a(t-1)}{g_1}\right), \tag{41}$$

where

$$G_a(t) = \sum_{i=1}^{n} R_i(t), \tag{42}$$

$$G_u(t) = \sum_{s=t_0}^{t} E(s) - G_a(t), \tag{43}$$

and

$$g_1 = \sum_{i=1}^{n} a_i \tau_i \left[1 - (1 + 100/\tau_i)\, e^{-100/\tau_i}\right], \tag{44}$$

$$g_0 = \exp\left(-\frac{\sum_{i=1}^{n} a_i \tau_i \left[1 - e^{-100/\tau_i}\right]}{g_1}\right). \tag{45}$$

$C(t)$ is the atmospheric stock/concentration of a given GHG, which is the sum of the pre-industrial stock $\underline{C}$ and the stock above pre-industrial. This stock above pre-industrial comprises $i = n$ boxes/reservoirs R_i (four for CO_2 and one for CH_4). Emissions E of the GHG in question are apportioned to box i according to its uptake fraction a_i and are removed at rate δ_i, which itself is a function of the decay timescale of the box τ_i and a state-dependent adjustment α, which

links the removal rate of the GHG from the atmosphere to current cumulative uptake G_u, warming $\Delta\overline{T_{AT}}$, and the stock above pre-industrial G_a. This state-dependent adjustment is a signature of the FaIR model and is capable of simulating positive and negative feedbacks in the gas cycle. r_0 is the strength of pre-industrial uptake from the atmosphere. The constants g_0 and g_1 are used for calibration of the state-dependent adjustment.

2.3 Radiative forcing and temperature

We also use FaIRv2.0.0 to convert atmospheric concentrations into effective radiative forcing and temperature change. This is also an update on META-2021, which used FaIRv1.0 (Millar et al., 2017) for CO_2 and Myhre et al. (2013) for CH_4. In general, the FaIR forcing equation includes logarithmic, square-root and linear terms:

$$F(t) = \sum_{x}^{\text{forcing agents}} \left\{ f_1^x \ln\left[\frac{C^x(t)}{\underline{C^x}}\right] + f_2^x \left[C^x(t) - \underline{C^x}\right] + f_3^x \left[\sqrt{C^x(t)} - \sqrt{\underline{C^x}}\right] \right\} + F_{\text{ext}}. \tag{46}$$

In META, the number of forcing agents $x = 2$, namely CO_2 and CH_4; F_{ext} is the sum of forcings from all other agents. For CO_2, the forcing relationship comprises the logarithmic and square-root terms only; for CH_4, just the square-root term (Leach et al., 2021).

From forcing, the increase in GMST is governed by a model comprising three heat boxes, which is one more than FaIRv1:

$$\Delta\overline{T_{AT}}(t) = \frac{1}{2}\left[\sum_{j=1}^{3} \Delta\overline{T_j}(t) + \sum_{j=1}^{3} \Delta\overline{T_j}(t-1)\right], \tag{47}$$

$$\Delta\overline{T_j}(t) = \Delta\overline{T_j}(t-1)e^{-1/d_j} + F(t)q_j\left(1 - e^{-1/d_j}\right), \tag{48}$$

where $\Delta\overline{T_j}$ is the temperature change for box j, e^{-1/d_j} is the thermal response decay factor, where d_j represents the thermal response timescale, and q_j is a radiative forcing coefficient.

3 Damages/economic module

3.1 Sea level rise

Sea level rise comprises a contribution from thermal expansion and melt from glaciers and small ice caps, $SLR_{\text{THERM}}(t)$, as well as a contribution from disintegration of the GIS and AIS:

$$\sum SLR(t) = SLR_{\text{THERM}}(t) + SLR_{\text{GIS}}(t) + SLR_{\text{AIS}}(t). \tag{49}$$

Sea level rise is defined relative to the year 2000 and $\sum SLR(0) = 0.04$m (Church and White, 2011). To model the contribution from thermal expansion and melt from glaciers and small ice caps, we follow Diaz and Keller (2016) in specifying SLR as a linear function of warming:

$$SLR_{\text{THERM}}(t) = (r_{\text{TE}} + r_{\text{GSIC}})\, \Delta\overline{T_{\text{AT}}}(t) + SLR_{\text{THERM}}(t-1), \tag{50}$$

where $r_{\text{TE}} = 0.00078$ and $r_{\text{GSIC}} = 0.00081$ parameterise the rates of SLR from thermal expansion and melt from glaciers and small ice caps respectively. Sea level rise from thermal expansion is parameterised such that 1°C warming results in a very long-term equilibrium increase of 0.5m (i.e., over the course of approximately 1000 years).

3.2 National temperature

We convert the increase in GMST relative to pre-industrial into the increase in national mean surface temperature using statistical downscaling. This procedure has been updated from META-2021 and now uses data from CMIP6. We subsequently add the effect of AMOC slowdown.

For country i, the change in mean surface temperature relative to pre-industrial is estimated using the following relationship:

$$\Delta T_{\text{AT}}(i,t) = \alpha(i) + \beta(i)\Delta\overline{T_{\text{AT}}}(t) + \Delta T_{\text{AT\_AMOC}}(i,t). \tag{51}$$

The coefficients α and β are estimated by regressing national mean surface temperature change from the CMIP6 dataset on corresponding GMST change. National mean surface temperature is constructed from the gridded CMIP6 output using population weights. We pool all available CMIP6 models and, for each model, we pool temperature changes from the historical runs with future projections on RCP2.6, RCP4.5, RCP7.0 and RCP8.5. We also tested quadratic and cubic

specifications of the national-global temperature change relationship, but the linear model was preferred based on the AIC and BIC; the relationship appears to be highly linear for all countries.

3.3 Damages and national income per capita

Income growth depends on exogenous drivers, as well as damages from changing temperatures and SLR (and from the summer monsoon in India, only). Post-damage income per capita in country i, $y(i,t)$, grows according to

$$y(i,t) = \overline{y}(i,t-1)\left[1 + g_{\mathrm{EX}}(i,t) + D_{\mathrm{TEMP}}(i,t)\right]\left[1 - D_{\mathrm{SLR}}(i,t)\right], \tag{52}$$

where $g_{\mathrm{EX}}(i,t)$ is an exogenous, country- and time-specific growth rate that is taken from the SSP database (O'Neill et al., 2014).[14] The SSP scenarios are only defined until 2100. To extend these scenarios until 2300, we follow a procedure described in Section 4.1.

$D_{\mathrm{TEMP}}(i,t)$ are temperature damages, which are given by

$$D_{\mathrm{TEMP}}(i,t) = \beta_1\left[T_{\mathrm{AT}}(i,t) - T_{\mathrm{AT}}(i,0)\right] + \beta_2\left[T_{\mathrm{AT}}(i,t) - T_{\mathrm{AT}}(i,0)\right]^2, \tag{53}$$

where the coefficients β_1 and β_2 are taken from the econometric analysis of Burke, Hsiang and Miguel (2015).

$D_{\mathrm{SLR}}(i,t)$ are SLR damages, which are given by

$$D_{\mathrm{SLR}}(i,t) = \theta(i)\sum SLR(t), \tag{54}$$

where $\theta(i)$ parameterises the cost to country i per unit SLR. We obtain SLR damages from Diaz's CIAM model (Diaz, 2016). We run CIAM to obtain estimates of national coastal damage/adaptation costs as a function of SLR in two scenarios, (i) no adaptation and (ii) optimal adaptation. We treat each country's adaptation decisions as uncertain and obtain a symmetrical triangular distribution for each $\theta(i)$ with a minimum corresponding to costs in (i) and a maximum corresponding to costs in (ii). We use costs/SLR in 2050 for the calibration, a simple approach facilitated by the fact that the relationship between the two is approximately linear over the 21st century (Diaz, 2016).

In India, there is an additional damage multiplier $D_{\mathrm{ISM}}(IND,t)$, so that national income per

[14] https://tntcat.iiasa.ac.at/SspDb

capita is given by

$$\begin{aligned} y(IND,t) &= \overline{y}(IND,t-1)\left[1+g_{\mathrm{EX}}(IND,t)+D_{\mathrm{TEMP}}(IND,t)\right]\times \\ &\quad \times\left[1-D_{\mathrm{SLR}}(IND,t)\right]\left[1-D_{\mathrm{ISM}}(IND,t)\right]. \end{aligned} \tag{55}$$

Following Belaia (2017), the ISM damage multiplier is given by

$$D_{\mathrm{ISM}}(t) = \begin{cases} D_{\mathrm{drought}}, & \overline{P}(t) \leq \overline{P}_{\mathrm{drought}}, \\ 0, & \overline{P}_{\mathrm{drought}} < \overline{P}(t) < \overline{P}_{\mathrm{flood}}, \\ D_{\mathrm{flood}}, & \overline{P}(t) \geq \overline{P}_{\mathrm{flood}}. \end{cases} \tag{56}$$

This structure implies that only extremely wet monsoon seasons and extremely dry monsoon seasons affect income in India, with the measure of precipitation being average rainfall for the monsoon season $\overline{P}(t)$. The drought threshold $\overline{P}_{\mathrm{drought}} = 2.8667$mm/day, while the equivalent flood threshold $\overline{P}_{\mathrm{flood}} = 7.6667$mm/day. Drought-related damages $D_{\mathrm{drought}} = 3.5\%$ of GDP, while flood-related damages $D_{\mathrm{flood}} = 0.85\%$. All these parameter values are taken from Belaia (2017).

The level of income per capita in the previous year, on which damages in the current year work, is given by

$$\overline{y}(i,t-1) = \varphi y_{\mathrm{EX}}(i,t-1) + (1-\varphi)\, y(i,t-1), \tag{57}$$

where $y_{\mathrm{EX}}(i,t-1)$ is counterfactual income per capita, also taken from the SSP database, $y(i,t-1)$ is the *actual* post-damage income per capita experienced, and φ parameterises the weight given to each. This specification enables us to explore two different interpretations of the empirical evidence on temperature damages, as well as convex combinations of them. The first interpretation is that temperatures impact the level of income in each year, in effect driving a wedge between what output is feasible given implicit factors of production and productivity, and what output is actually achieved. This has been the traditional approach in climate economics, e.g., in Nordhaus' DICE model. The production possibilities frontier is assumed to evolve exogenously. Such 'levels' damages correspond with $\varphi = 1$. The second interpretation is that temperatures impact the growth rate of income by directly impacting the accumulation of factors of production and/or by impacting productivity growth (Dietz and Stern, 2015). Such 'growth' damages correspond with $\varphi = 0$. The persistence of damages and the extent to which they impact growth/levels is an active area of debate in climate economics (Newell, Prest and Sexton, 2021; Casey, Fried and Goode, 2023; Klenow, Nath

and Ramey, 2023). We calibrate φ on the long-run projections of Klenow, Nath and Ramey (2023), which suggest that warming on the RCP8.5 scenario would reduce global GDP by 11.5% by 2100. Given estimates of temperature, SLR and ISM damages, this implies $\varphi = 0.25$.

3.4 Utility and welfare

Post-damage national income per capita is first converted into consumption per capita using a country-specific but time-invariant savings rate,

$$c(i,t) = [1 - s(i)]\, y(i,t), \tag{58}$$

where the country savings rates $s(i)$ are calibrated on observed national savings rates averaged over the period 2005-2015, using World Bank data. Savings data are missing for many countries, in which case we impute the global average, also obtained from the World Bank. This specification assumes savings are exogenous and do not respond to changing income prospects. Fully endogenous savings are computationally infeasible in a model with this much complexity and detail. The limitations of assuming constant/exogenous savings have been discussed in the literature, e.g., Golosov et al. (2014). Small to moderate climate damages do not appear to shift savings rates measurably.

Consumption is converted into utility using a standard, constant-elasticity-of-substitution representation,

$$u(i,t) = \frac{c(i,t)^{1-\eta}}{1-\eta}, \tag{59}$$

where η is the elasticity of marginal utility of consumption.

To compute overall welfare, we specify a discounted classical/total utilitarian social welfare functional. We begin by calculating welfare for each country i:

$$W(i) = \sum_{t=2020}^{T} (1+\rho)^{-t}\, u(i,t) L(i,t), \tag{60}$$

where ρ is the utility discount rate, a.k.a. the pure rate of time preference. Discounted, population-adjusted current period utility is then summed over the whole modelling horizon to obtain total welfare. Population data are exogenous and taken from the SSP scenarios.

Global welfare follows naturally as the sum of welfare across all countries i:

$$W = \sum_{i} W(i) \tag{61}$$

3.5 Non-market damages

The above damages from temperature, SLR and the ISM can be regarded as 'market' damages. Market damages are those climate damages affecting economic activity mediated by money. Market damages do not include estimates of the welfare cost of climate change outside markets, for example loss of human life (McDuffie et al., 2023) or damages to ecosystems that can be priced at people's willingness to pay (WTP) to preserve those ecosystems' existence. 'Non-market' damages are more uncertain than their market counterparts, but in many IAMs they occupy a substantial share of total welfare damages from climate change (e.g. Nordhaus and Boyer, 2000; Rennert et al., 2022).

We use the non-market damage module of the MERGE IAM (Manne and Richels, 2005), with an updated calibration derived from Howard and Sterner (2017). The MERGE model places particular emphasis on the representation of non-market damages, with a WTP measure that depends on both income and temperature. While the parameters of the MERGE non-market damage module are speculative, its use of an S-shaped elasticity of WTP with respect to income is theoretically coherent.

Like the MERGE model, the damage function meta-analysis by Howard and Sterner (2017) assumes that damages grow quadratically with warming from a pre-industrial baseline. Under their preferred model, total damages as a percent of GDP (including market and non-market impacts) follow $0.595\Delta\overline{T_{AT}}(t)^2$. Considering only damage functions that exclude non-market damages, their key coefficient is reduced by 0.487.[15] We use this as evidence that non-market damages follow $0.487\Delta\overline{T_{AT}}(t)^2$. As in Howard and Sterner (2017), we increase this coefficient by 25%, to 0.609, to account for potential omitted (non-catastrophic) damages. This gives a 90% increase in WTP relative to Manne and Richels (2005). At 2.5°C warming, WTP is 3.8% of GDP, compared to 2.0% in the original MERGE calibration (see Figure 6).

This WTP applies at high incomes. MERGE provides a model to link WTP to income, which we maintain. At \$25k/capita, WTP to avoid 2.5°C warming is held at 1%. As income increases above that level, WTP asymptotically approaches the non-market damages from Howard and Sterner (2017). WTP to avoid warming as a function of income is shown in Figure 7.

We calculate this WTP measure at a national level. The non-market damage multiplier, or

[15] This coefficient comes from table 2, column 3 of Howard and Sterner (2017). While their preferred model is column 4, that model has a market-only reduction of 0.622, larger than the total damage coefficient. Columns 3 and 4 estimate identical values for the total damage coefficient, so we use the more conservative value.

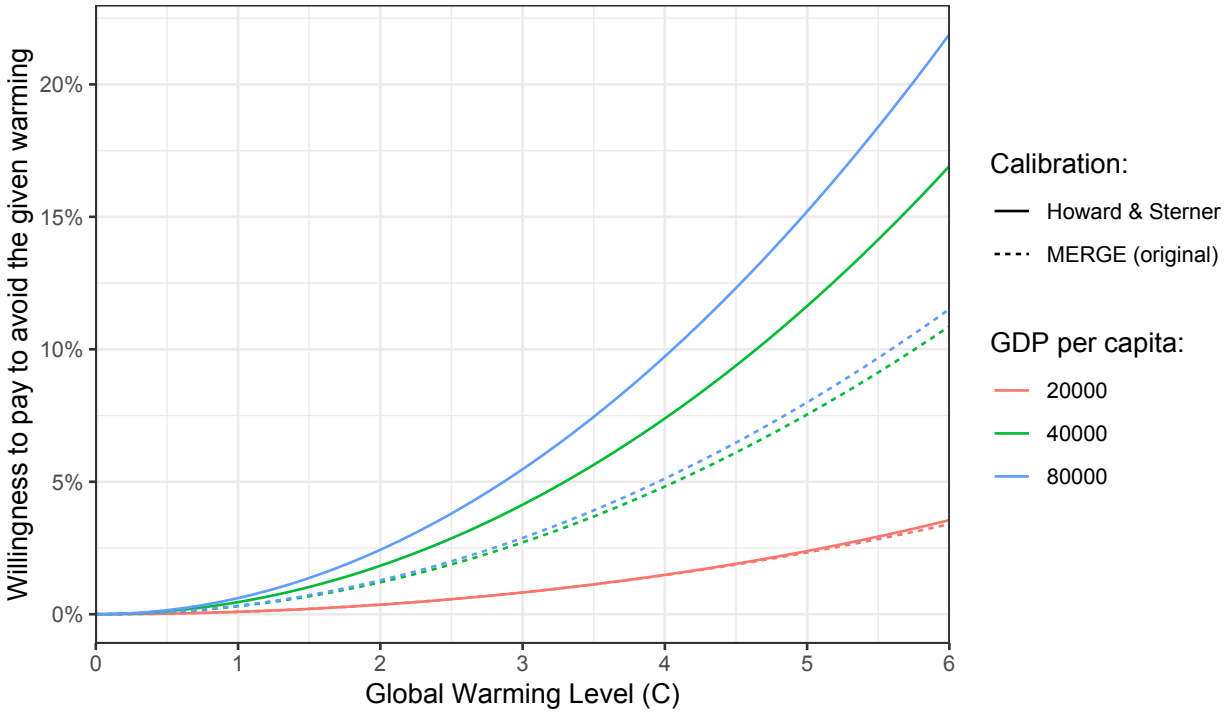

Figure 6: Willingness to pay to avoid levels of warming, split by levels of income. The original and updated calibrations are shown.

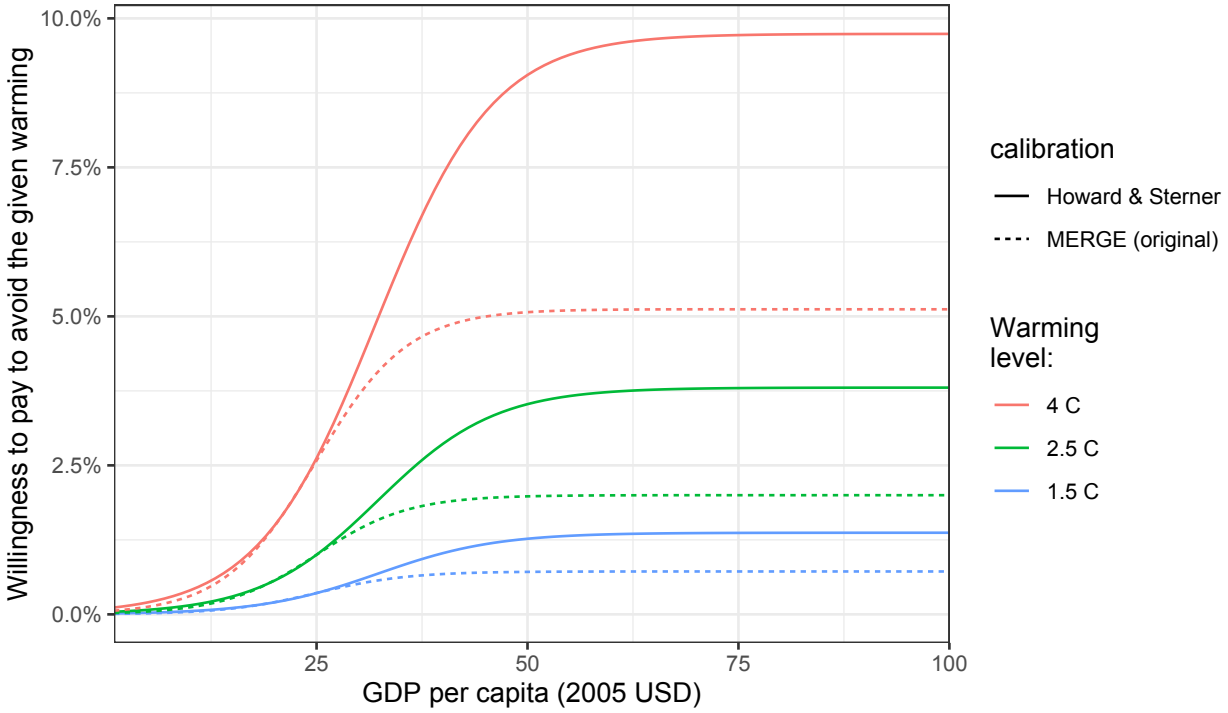

Figure 7: Willingness to pay to avoid 1.5, 2.5, and 4 °C, as a function of income, under the original and updated calibrations.

economic loss function, is

$$D_{\mathrm{NM}}(i,t) = \left[1 - \left(\left(\frac{\Delta\overline{T_{\mathrm{AT}}}(t)}{\Delta T_{\mathrm{cat}}}\right)^2 - \left(\frac{\Delta\overline{T_{\mathrm{AT}}}(0)}{\Delta T_{\mathrm{cat}}}\right)^2\right)\right]^{h(i,t)}. \tag{62}$$

where $\overline{T_{\mathrm{AT}}}(0)$ is the temperature in the baseline period, which is taken to be 2010.

This is a hockey-stick function embodying the assumption that non-market damages can increase rapidly as temperatures become more extreme. ΔT_{cat} is a catastrophic warming parameter set to 12.82°C, which people are assumed to be willing to avoid at any cost[16]. $h(i,t)$ is the hockey-stick parameter, which depends on country income per capita ($y(i,t)$):

$$h(i,t) = \min\left[\frac{\log\left[1 - \frac{D_{\mathrm{ref}}}{1+100\exp\left[-WTP_{\mathrm{ref}}y(i,t)\right]}\right]}{\log\left[1 - \left(\Delta T_{\mathrm{ref}}/\Delta T_{\mathrm{cat}}\right)^2\right]}, 1\right], \tag{63}$$

where

$WTP_{\mathrm{ref}} = 0.143$	WTP 1% of GDP to avoid reference warming at \$25k/capita
$D_{\mathrm{ref}} = 0.038$	WTP loss at reference warming
$\Delta T_{\mathrm{ref}} = 2.5\,\mathrm{C}$	WTP reference warming

The non-market damage multiplier is applied to country-level utility:

$$u(i,t) = u\left(D_{\mathrm{NM}}(i,t)c(i,t)\right)$$

for utility function $u(\cdot)$ as specified above.

3.6 Marginal and total damages

The marginal damage cost/social cost of carbon or methane along a particular scenario of emissions, income and population is the difference in welfare caused by a marginal emission of the gas, normalised by the marginal welfare value of a unit of consumption in the base year:

$$\mathrm{SCC}(t) = \frac{\partial W/\partial E(t)}{\partial W/\partial c(t)}. \tag{64}$$

[16]The catastrophic warming temperature is derived from the assumption that economic losses rise quadratically according to the Howard and Sterner (2017) calibration.

To calculate the numerator, we run the model twice with identical assumptions, the second time with an additional pulse of emissions. Let ϑ_m represent a vector of parameter values from the model, representing in abstract form the many parameters described above. These are in most cases random draws from a distribution, including individual tipping event realisations. Then we calculate

$$\left[\frac{\partial W}{\partial E(t)}\right]_m = \frac{W[E(t) + \Delta_E(t), \vartheta_m] - W[E(t), \vartheta_m]}{\Delta_E(t)}, \tag{65}$$

where Δ_E is the emissions pulse. We focus on an emissions pulse in 2020.

The denominator of (64), $\partial W/\partial c(t)$, depends on the consumption level of the normalising agent. We define this as the global average individual, i.e., global mean consumption per capita:

$$\bar{c}(t, \theta_m) = \frac{\sum_i c(i, t, \vartheta_m) L(i, t)}{\sum_i L(i, t)}. \tag{66}$$

Note that this is also uncertain and depends on the vector of random parameters. Differentiating the utility function, we then have

$$\left[\frac{\partial W}{\partial c(t)}\right]_m = \bar{c}(i, t, \theta_m)^{-\eta}. \tag{67}$$

We focus on a base year of 2020. We then calculate the negative of the ratio of Equations (65) and (67) for each draw of random parameters m and take expectations over all draws. The numeraire in the model is year 2010 US dollars, corresponding to the year in which GDP is initialised. We inflate our reported SCC values to year 2020 US dollars using a factor of 1.2, based on data from World Bank (2020).[17]

4 Supporting analysis

4.1 Extending the SSP scenarios beyond 2100

To estimate post-2100 income and population along the SSP scenarios, we fit a model to the available pre-2100 SSP scenario data and use the fitted model to extrapolate. The same model is applied to both income and population and is defined in terms of growth rates. The model postulates that changes in pre-2100 income and population growth rates are explained by a rate of convergence and a rate of decay.

[17] The inflation factor is 1.2 whether one uses the Consumer Price Index or the GDP deflator.

The model is as follows:

$$\text{Growth}(i,t) = (1-\beta-\delta)\text{Growth}(i,t-1) + \delta\text{MeanGrowth}(t-1), \tag{68}$$

where δ is the rate of convergence, β is the decay rate and

$$\text{MeanGrowth}(t-1) = \sum_i \frac{\text{Population}(i,2015)}{\sum_j \text{Population}(j,2015)}\text{Growth}(i,t-1). \tag{69}$$

Below, we write this as $\text{Growth}(\cdot,t-1)\cdot w$, where w is the vector of global population shares for each country.

SSP data are not available in every year, so fitting Eq. (68) requires a model with dynamics. We use a two-step approach, fitting the model using Stan, a computational Bayes system. The first step uses the available data directly, fitting

$$\text{Growth}(i,s) \sim \mathcal{N}\left([1-\Delta t(\beta+\delta)]\text{Growth}(i,s-1) + \Delta t\delta\text{MeanGrowth}(s-1), \sigma_i\right), \tag{70}$$

where s is a time step, Δt is the number of years between time steps, and country i has uncertainty σ_i. We apply a prior that both β and δ are between 0 and 0.5.

Next, we fit the full model, using the results of the simplified model to improve the Bayesian model convergence. In this case, for a given Markov chain Monte Carlo draw of β and δ, we calculate the entire time series:

$$\widehat{\text{Growth}}(i,t) \sim \mathcal{N}\left((1-\beta-\delta)\widehat{\text{Growth}}(i,t-1) + \delta\left[\widehat{\text{Growth}}(\cdot,t-1)\cdot w_\cdot\right], \sigma_i\right) \tag{71}$$

starting with $\widehat{\text{Growth}}(i,2015)$ as reported in the SSP dataset.

The probability evaluation is over both the performance of the fit and the priors:

$$\begin{aligned}
\text{Growth}(i,s) &\sim \mathcal{N}\left(\widehat{\text{Growth}}(i,t(s)), \sigma_i\right)\\
\beta &\sim \mathcal{N}\left(\mu_\beta, \sigma_\beta\right)\\
\delta &\sim \mathcal{N}\left(\mu_\delta, \sigma_\delta\right)\\
\log\sigma_i &\sim \mathcal{N}\left(\mu_{\sigma,i}, \sigma_{\sigma,i}\right)
\end{aligned}$$

where μ is the mean estimate of the corresponding parameter and σ is the standard deviation across

its uncertainty. The prior for σ_i is defined as a log-normal, centered on the mean of the estimates of log σ_i. The estimates for each SSP are shown in Table 4.

Table 4: Estimated convergence and decay rates for extrapolation of growth of GDP per capita and population in the SSP socio-economic scenarios beyond 2100

SSP	Variable	δ	β
1	GDP per capita	0.006205028	0.005930520
1	Population	0.008967453	0.005215835
2	GDP per capita	0.004190444	0.007228942
2	Population	0.001276993	0.011064426
3	GDP per capita	0.006273030	0.009597363
3	Population	0.001064697	0.007688331
4	GDP per capita	0.006895296	0.009651277
4	Population	0.001867587	0.003461600
5	GDP per capita	0.007766807	0.003843256
5	Population	0.003470952	0.004305310

References

Alley, Richard B, John Thomas Andrews, Julia Brigham-Grette, GKC Clarke, Kurt M Cuffey, JJ Fitzpatrick, S Funder, SJ Marshall, GH Miller, JX Mitrovica, et al. 2010. "History of the Greenland Ice Sheet: paleoclimatic insights." *Quaternary Science Reviews*, 29(15-16): 1728–1756.

Anthoff, David, Francisco Estrada, and Richard SJ Tol. 2016. "Shutting down the thermohaline circulation." *American Economic Review: Papers and Proceedings*, 106(5): 602–06.

Archer, D. 2015. "A model of the methane cycle, permafrost, and hydrology of the Siberian continental margin." *Biogeosciences*, 12(10): 2953–2974.

Archer, David, Bruce Buffett, and Victor Brovkin. 2009. "Ocean methane hydrates as a slow tipping point in the global carbon cycle." *Proceedings of the National Academy of Sciences*, 106(49): 20596–20601.

Bahn, Olivier, Neil R Edwards, Reto Knutti, and Thomas F Stocker. 2011. "Energy policies avoiding a tipping point in the climate system." *Energy Policy*, 39(1): 334–348.

Belaia, Mariia. 2017. "Integrated assessment of climate tipping points." PhD diss. Universität Hamburg Hamburg.

Belaia, Mariia, Michael Funke, and Nicole Glanemann. 2017. "Global warming and a potential tipping point in the atlantic thermohaline circulation: the role of risk aversion." *Environmental and Resource Economics*, 67(1): 93–125.

Burke, Marshall, Solomon M Hsiang, and Edward Miguel. 2015. "Global non-linear effect of temperature on economic production." *Nature*, 527: 235–239.

Cai, Yongyang, Timothy M Lenton, and Thomas S Lontzek. 2016. "Risk of multiple interacting tipping points should encourage rapid CO2 emission reduction." *Nature Climate Change*, 6(5): 520.

Casey, Gregory, Stephie Fried, and Ethan Goode. 2023. "Projecting the impact of rising temperatures: The role of macroeconomic dynamics." *IMF Economic Review*, 1–31.

Ceronsky, Megan, David Anthoff, Cameron Hepburn, and Richard SJ Tol. 2011. "Checking the price tag on catastrophe: the social cost of carbon under non-linear climate response." ESRI working paper.

Church, John A, and Neil J White. 2011. "Sea-level rise from the late 19th to the early 21st century." *Surveys in Geophysics*, 32(4-5): 585–602.

Diaz, Delavane, and Klaus Keller. 2016. "A potential disintegration of the West Antarctic Ice Sheet: implications for economic analyses of climate policy." *American Economic Review: Papers and Proceedings*, 106(5): 607–11.

Diaz, Delavane B. 2016. "Estimating global damages from sea level rise with the Coastal Impact and Adaptation Model (CIAM)." *Climatic Change*, 137(1-2): 143–156.

Dietz, Simon, and Felix Koninx. 2022. "Economic impacts of melting of the Antarctic Ice Sheet." *Nature Communications*, 13(1): 5819.

Dietz, Simon, and Nicholas Stern. 2015. "Endogenous growth, convexity of damages and climate risk: how Nordhaus' framework supports deep cuts in carbon emissions." *Economic Journal*, 125(583): 574–620.

Dietz, Simon, James Rising, Thomas Stoerk, and Gernot Wagner. 2021. "Economic impacts of tipping points in the climate system." *Proceedings of the National Academy of Sciences*, 118(34): e2103081118.

Frieler, Katja, Peter U Clark, Feng He, Christo Buizert, Ronja Reese, Stefan RM Ligtenberg, Michiel R Van Den Broeke, Ricarda Winkelmann, and Anders Levermann. 2015. "Consistent evidence of increasing Antarctic accumulation with warming." *Nature Climate Change*, 5(4): 348–352.

Garbe, Julius, Torsten Albrecht, Anders Levermann, Jonathan F Donges, and Ricarda Winkelmann. 2020. "The hysteresis of the Antarctic ice sheet." *Nature*, 585(7826): 538–544.

Golosov, Mikhail, John Hassler, Per Krusell, and Aleh Tsyvinski. 2014. "Optimal taxes on fossil fuel in general equilibrium." *Econometrica*, 82(1): 41–88.

Gosling, Simon N. 2013. "The likelihood and potential impact of future change in the large-scale climate-earth system on ecosystem services." *Environmental Science & Policy*, 27(1): S15–S31.

Hoegh-Guldberg, O., D. Jacob, M. Taylor, M. Bindi, S. Brown, I. Camilloni, A. Diedhiou, R. Djalante, K.L. Ebi, F. Engelbrecht, J. Guiot, Y. Hijioka, S. Mehrotra, A. Payne, S.I. Seneviratne, A. Thomas, R. Warren, and G. Zhou. 2018. "Impacts of 1.5°C Global Warming on Natural and Human Systems." In *Global Warming of 1.5°C. An IPCC Special Report on the impacts of global warming of 1.5°C above pre-industrial levels and related global greenhouse gas emission pathways, in the context of strengthening the global response to the threat of climate change, sustainable development, and efforts to eradicate poverty.* , ed. V. Masson-Delmotte, P. Zhai, H.-O. Pörtner, D. Roberts, J. Skea, P.R. Shukla, A. Pirani, W. Moufouma-Okia, C. Péan, R. Pidcock, S. Connors, J.B.R. Matthews, Y. Chen, X. Zhou, M.I. Gomis, E. Lonnoy, T. Maycock, M. Tignor and T. Waterfield. in press.

Hope, Chris, and Kevin Schaefer. 2016. "Economic impacts of carbon dioxide and methane released from thawing permafrost." *Nature Climate Change*, 6(1): 56–59.

Howard, Peter H, and Thomas Sterner. 2017. "Few and not so far between: a meta-analysis of climate damage estimates." *Environmental and Resource Economics*, 68(1): 197–225.

Ikefuji, Masako, Jan R Magnus, and Hiroaki Sakamoto. 2014. "The effect of health benefits on climate change mitigation policies." *Climatic Change*, 126(1-2): 229–243.

Keller, Klaus, Benjamin M Bolker, and David F Bradford. 2004. "Uncertain climate thresholds and optimal economic growth." *Journal of Environmental Economics and Management*, 48(1): 723–741.

Kessler, Louise. 2017. "Estimating the economic impact of the permafrost carbon feedback." *Climate Change Economics*, 8(02): 1750008.

Klenow, P, I Nath, and V Ramey. 2023. "How much will global warming cool global growth." Working paper.

Kriegler, Elmar, Jim W Hall, Hermann Held, Richard Dawson, and Hans Joachim Schellnhuber. 2009*a*. "Imprecise probability assessment of tipping points in the climate system." *Proceedings of the National Academy of Sciences*, 106(13): 5041–5046.

Kriegler, Elmar, Jim W. Hall, Hermann Held, Richard Dawson, and Hans Joachim Schellnhuber. 2009*b*. "Imprecise probability assessment of tipping points in the climate system." *Proceedings of the National Academy of Sciences*, 106(13): 5041–5046.

Leach, N. J., S. Jenkins, Z. Nicholls, C. J. Smith, J. Lynch, M. Cain, T. Walsh, B. Wu, J. Tsutsui, and M. R. Allen. 2021. "FaIRv2.0.0: a generalized impulse response model for climate uncertainty and future scenario exploration." *Geoscientific Model Development*, 14(5): 3007–3036.

Lempert, Robert J, Alan H Sanstad, and Michael E Schlesinger. 2006. "Multiple equilibria in a stochastic implementation of DICE with abrupt climate change." *Energy Economics*, 28(5-6): 677–689.

Lenton, Timothy M, and Juan-Carlos Ciscar. 2013. "Integrating tipping points into climate impact assessments." *Climatic Change*, 117(3): 585–597.

Levermann, Anders, Ricarda Winkelmann, Torsten Albrecht, Heiko Goelzer, Nicholas R Golledge, Ralf Greve, Philippe Huybrechts, Jim Jordan, Gunter Leguy, Daniel Martin, et al. 2020. "Projecting Antarctica's contribution to future sea level rise from basal ice shelf melt using linear response functions of 16 ice sheet models (LARMIP-2)." *Earth System Dynamics*, 11(1): 35–76.

Li, Can, Chris McLinden, Vitali Fioletov, Nickolay Krotkov, Simon Carn, Joanna Joiner, David Streets, Hao He, Xinrong Ren, Zhanqing Li, et al. 2017. "India is overtaking China as the world's largest emitter of anthropogenic sulfur dioxide." *Scientific Reports*, 7(1): 14304.

Link, P Michael, and Richard SJ Tol. 2004. "Possible economic impacts of a shutdown of the thermohaline circulation: an application of FUND." *Portuguese Economic Journal*, 3(2): 99–114.

Link, P Michael, and Richard SJ Tol. 2011. "Estimation of the economic impact of temperature changes induced by a shutdown of the thermohaline circulation: an application of FUND." *Climatic Change*, 104(2): 287–304.

Manne, Alan S, and Richard G Richels. 2005. "MERGE: an integrated assessment model for global climate change." In *Energy and environment*. 175–189. Springer.

McDuffie, Erin E., Marcus C. Sarofim, William Raich, Melanie Jackson, Henry Roman, Karl Seltzer, Barron H. Henderson, Drew T. Shindell, Mei Collins, Jim Anderton, Sarah Barr, and Neal Fann. 2023. "The Social Cost of Ozone-Related Mortality Impacts From Methane Emissions." *Earth's Future*, 11(9): e2023EF003853.

Millar, Richard J, Zebedee R Nicholls, Pierre Friedlingstein, and Myles R Allen. 2017. "A modified impulse-response representation of the global near-surface air temperature and atmospheric concentration response to carbon dioxide emissions." *Atmospheric Chemistry and Physics*, 17(11): 7213–7228.

Moss, Richard H, Jae A Edmonds, Kathy A Hibbard, Martin R Manning, Steven K Rose, Detlef P Van Vuuren, Timothy R Carter, Seita Emori, Mikiko Kainuma, Tom Kram, et al. 2010. "The next generation of scenarios for climate change research and assessment." *Nature*, 463(7282): 747–756.

Myhre, G., D. Shindell, F.-M. Bréon, W. Collins, J. Fuglestvedt, J. Huang, D. Koch, J.-F. Lamarque, D. Lee, B. Mendoza, T. Nakajima, A. Robock, G. Stephens, T. Takemura, and H. Zhang. 2013. "Anthropogenic and natural radiative forcing: supplementary material." In *Climate Change 2013: The Physical Science Basis. Contribution of Working Group I to the Fifth Assessment Report of the Intergovernmental Panel on Climate Change.* , ed. T.F. Stocker, D. Qin, G.-K. Plattner, M. Tignor, S.K. Allen, J. Boschung, A. Nauels, Y. Xia, V. Bex and P.M. Midgley, 8SM–1–8SM–44. IPCC.

Newell, Richard G, Brian C Prest, and Steven E Sexton. 2021. "The GDP-temperature relationship: implications for climate change damages." *Journal of Environmental Economics and Management*, 108: 102445.

Nordhaus, William. 2019. "Economics of the disintegration of the Greenland ice sheet." *Proceedings of the National Academy of Sciences*, 116(25): 12261–12269.

Nordhaus, William D, and Joseph Boyer. 2000. *Warming the World: Economic Models of Global Warming.* MIT Press (MA).

O'Neill, Brian C, Elmar Kriegler, Keywan Riahi, Kristie L Ebi, Stephane Hallegatte, Timothy R Carter, Ritu Mathur, and Detlef P van Vuuren. 2014. "A new scenario framework for climate change research: the concept of shared socioeconomic pathways." *Climatic Change*, 122(3): 387–400.

Rennert, Kevin, Frank Errickson, Brian C Prest, Lisa Rennels, Richard G Newell, William Pizer, Cora Kingdon, Jordan Wingenroth, Roger Cooke, Bryan Parthum, et al. 2022. "Comprehensive evidence implies a higher social cost of CO2." *Nature*, 610(7933): 687–692.

Robinson, Alexander, Reinhard Calov, and Andrey Ganopolski. 2012. "Multistability and critical thresholds of the Greenland ice sheet." *Nature Climate Change*, 2(6): 429–432.

Schewe, Jacob, and Anders Levermann. 2012. "A statistically predictive model for future monsoon failure in India." *Environmental Research Letters*, 7(4): 044023.

Schlesinger, Michael E, Jianjun Yin, Gary Yohe, Natalia G Andronova, Sergey Malyshev, and Bin Li. 2006. "Assessing the risk of a collapse of the Atlantic thermohaline circulation." In *Avoiding Dangerous Climate Change*. 37–47. Cambridge University Press, Cambridge, UK.

Shakhova, NE, VA Alekseev, and IP Semiletov. 2010. "Predicted methane emission on the East Siberian shelf." *Doklady Earth Sciences*, 430(2): 190–193.

Stocker, T.F., D. Qin, G.-K. Plattner, L.V. Alexander, S.K. Allen, N.L. Bindoff, F.-M. Bréon, J.A. Church, U. Cubasch, S. Emori, P. Forster, P. Friedlingstein, N. Gillett, J.M. Gregory, D.L. Hartmann, E. Jansen, B. Kirtman, R. Knutti, K. Krishna-Kumar, P. Lemke, J. Marotzke, V. Masson-Delmotte, G.A. Meehl, I.I. Mokhov, S. Piao, V. Ramaswamy, D. Randall, M. Rhein, M. Rojas, C. Sabine, D. Shindell, L.D. Talley, D.G. Vaughan, and S.-P. Xie. 2013. "Technical Summary." In *Climate Change 2013: The Physical Science Basis. Contribution of Working Group I to the Fifth Assessment Report of the Intergovernmental Panel on Climate Change*. , ed. T.F. Stocker, D. Qin, G.-K. Plattner, M. Tignor, S.K. Allen, J. Boschung, A. Nauels, Y. Xia, V. Bex and P.M. Midgley, 33–115. Cambridge, United Kingdom and New York, NY, USA:Cambridge University Press.

Whiteman, Gail, Chris Hope, and Peter Wadhams. 2013. "Climate science: vast costs of Arctic change." *Nature*, 499(7459): 401–403.

World Bank. 2020. "World Development Indicators."

Yumashev, Dmitry, Chris Hope, Kevin Schaefer, Kathrin Riemann-Campe, Fernando Iglesias-Suarez, Elchin Jafarov, Eleanor J Burke, Paul J Young, Yasin Elshorbany, and Gail Whiteman. 2019. "Climate policy implications of nonlinear decline of Arctic land permafrost and other cryosphere elements." *Nature Communications*, 10(1): 1900.